(1)

AFOSR-TR- 89-0365

Final Technical Report
for
AFOSR Grant No. 86-0051

FUNDAMENTAL STUDIES OF THE MECHANICAL BEHAVIOR OF MICROELECTRONIC THIN FILM MATERIALS

Submitted to :

Department of the Air Force
Directorate of Electronic and Materials Sciences
Air Force of Office of Scientific Research
Bolling Air Force Base, Building 410
Washington D.C. 20332

Attention: Drs. Alan H. Rosenstein and Gerald Witt

Submitted by:

Professor William D. Nix, Principal Investigator
Department of Materials Science and Engineering
Stanford University, Stanford, CA 94305

January 1989

UNCLASSIFIED
SECURITY CLASSIFICATION OF THIS PAGE

REPORT DOCUMENTATION PAGE

Form Approved OMB No. 0704-0188

1a. REPORT SECURITY CLASSIFICATION: UNCLASSIFIED	1b. RESTRICTIVE MARKINGS
2a. SECURITY CLASSIFICATION AUTHORITY	3. DISTRIBUTION / AVAILABILITY OF REPORT: Approved For Public Release; Unlimited
2b. DECLASSIFICATION / DOWNGRADING SCHEDULE	
4. PERFORMING ORGANIZATION REPORT NUMBER(S)	5. MONITORING ORGANIZATION REPORT NUMBER(S): AFOSR-TR- 89-0365
6a. NAME OF PERFORMING ORGANIZATION: STANFORD Univ. / 6b. OFFICE SYMBOL (If applicable): MSE	7a. NAME OF MONITORING ORGANIZATION: AFOSR/NE
6c. ADDRESS (City, State, and ZIP Code): DEPT. OF MSE, STANFORD, CA. 94305	7b. ADDRESS (City, State, and ZIP Code): BLDG. 410, BAFB, DC 20332
8a. NAME OF FUNDING / SPONSORING ORGANIZATION: AFOSR / 8b. OFFICE SYMBOL (If applicable): NE	9. PROCUREMENT INSTRUMENT IDENTIFICATION NUMBER: AFOSR-86-0051
8c. ADDRESS (City, State, and ZIP Code): Bldg. 410, BAFB, DC 20332	10. SOURCE OF FUNDING NUMBERS: PROGRAM ELEMENT NO 61102F; PROJECT NO. 2306; TASK NO A1; WORK UNIT ACCESSION NO —

11. TITLE (Include Security Classification)
(U) FUNDAMENTAL STUDIES OF THE MECHANICAL PROPERTIES OF MICROELECTRONIC THIN FILM MATERIALS

12. PERSONAL AUTHOR(S): W.D. Nix

13a. TYPE OF REPORT	13b. TIME COVERED	14. DATE OF REPORT (Year, Month, Day)	15. PAGE COUNT
FINAL	FROM JAN 86 TO DEC 88	JAN. 1989	44

16. SUPPLEMENTARY NOTATION

17. COSATI CODES			18. SUBJECT TERMS (Continue on reverse if necessary and identify by block number)
FIELD	GROUP	SUB-GROUP	Thin Films, Mechanical Behavior, Microelectronics
11.06			
20.12			

19. ABSTRACT (Continue on reverse if necessary and identify by block number)

It is appropriate to note that before this research program began, very little work had been done in universities on the mechanical properties of microelectronic thin film materials. As a result, much of our early work involved the development of experimental techniques, such as sub-micron indentation and wafer curvature measurement, to study stresses and mechanical properties of thin films on substrates. Interest in these developments is indicated by the accepted publications and invited oral presentations listed at the end of this report. The recent MRS Symposium on "Thin Films: Stresses and Mechanical Properties" was an outgrowth of the research work started under this grant.

(over)

20. DISTRIBUTION / AVAILABILITY OF ABSTRACT: ☒ UNCLASSIFIED/UNLIMITED ☐ SAME AS RPT ☐ DTIC USERS	21. ABSTRACT SECURITY CLASSIFICATION: Unc.
22a. NAME OF RESPONSIBLE INDIVIDUAL: A.H. ROSENSTEIN	22b. TELEPHONE (Include Area Code): (202) 767-4933 / 22c. OFFICE SYMBOL: NE

DD Form 1473, JUN 86 — Previous editions are obsolete. — SECURITY CLASSIFICATION OF THIS PAGE

Throughout this program we have been interested in the mechanical properties of all kinds of microelectronic thin film materials. We have studied stresses and mechanical properties in interconnect metals, passivation glasses and semiconductors. Most of the experimental work to date has focused on interconnect metals and passivation glasses More work will be done on semiconductors in the follow-on grant. The wafer curvature technique, that has proved so useful in the study of metals and passivation glasses, will be used in the study of semiconductor thin films. In the present report we present an up-date on our work on the wafer curvature technique. This includes a description of the factors that control the sensitivity of this technique as well as a report on the efforts we have made to develop better facilities for making these measurements.

The films present in integrated circuit structures have irregular geometries that complicate the understanding of mechanical behavior. In particular, it is necessary to have an understanding of the stresses that exist in these structures. Here we report the results of a comprehensive study of the stresses in interconnect lines bonded to substrates. The results are presented in a form that should permit them to be used for a wide variety of thin film stress problems.

Table of Contents

I. SUMMARY

A fundamental study of the mechanical properties of microelectronic thin film materials has been conducted at Stanford University. The work was supported by AFOSR Grant No. 86-0051. In this final technical report we summarize all of the findings of this research program by citing the papers and oral presentations that have resulted from the work. The interested reader is referred to these published papers for detailed descriptions of this work. In the following sections, we describe some of the work, done in the last year, that has not yet appeared in print. Much of the recent progress described in this report will serve as a basis for the work of the follow-on grant.

It is appropriate to note that before this research program began, very little work had been done in universities on the mechanical properties of microelectronic thin film materials. As a result, much of our early work involved the development of experimental techniques, such as sub-micron indentation and wafer curvature measurement, to study stresses and mechanical properties of thin films on substrates. Interest in these developments is indicated by the accepted publications and invited oral presentations listed at the end of this report. The recent MRS Symposium on "Thin Films: Stresses and Mechanical Properties" was an outgrowth of the research work started under this grant.

Throughout this program we have been interested in the mechanical properties of all kinds of microelectronic thin film materials. We have studied stresses and mechanical properties in interconnect metals, passivation glasses and semiconductors. Most of the experimental work to date has focused on interconnect metals and passivation glasses. More work will be done on semiconductors in the follow-on grant. The wafer curvature technique, that has proved so useful in the study of metals and passivation glasses, will be used in the study of semiconductor thin films. In the present report we present an up-date on our work on the wafer curvature technique. This includes a description of the factors that control the sensitivity of this technique as well as a report on the efforts we have made to develop better facilities for making these measurements.

Final Technical Report
for
AFOSR Grant No. 86-0051

FUNDAMENTAL STUDIES OF THE MECHANICAL BEHAVIOR OF MICROELECTRONIC THIN FILM MATERIALS

Submitted to :

Department of the Air Force
Directorate of Electronic and Materials Sciences
Air Force of Office of Scientific Research
Bolling Air Force Base, Building 410
Washington D.C. 20332

Attention: Drs. Alan H. Rosenstein and Gerald Witt

Submitted by:

Professor William D. Nix, Principal Investigator
Department of Materials Science and Engineering
Stanford University, Stanford, CA 94305

January 1989

This research was supported by the Air Force of Scientific Research (AFOSC) under Grant No. AFOSR-86-0051. Approved for public release; distribution unlimited.

A. Some Issues Concerning Curvature of a Plate Relevant To Thin-Film Stress Analysis

(F. von Preissig)

1. Introduction

Thin solid films of many kinds, deposited or grown onto substrates, are used in today's microelectronic devices and for other purposes. Mechanical stresses in these films arise from various causes, including thermal expansion differences between film and substrate materials, the physical nature of the as-deposited material, and chemical or structural changes occurring in the films upon processing after deposition. These stresses can lead to cracking or delamination of the films and can induce dislocation formation in the substrate. The study of film stress is also of interest as a probe of the physico-chemical nature of the film material.

In order to experimentally determine mechanical stresses in thin films on substrates, it is common practice to use the formula

$$C = \frac{1}{R} = \frac{6(1-\nu)\sigma h}{Et^2}\ , \qquad (1)$$

where

C = curvature of substrate; R = radius of curvature
E = Young's modulus of substrate
ν = Poisson's ratio of substrate
h = film thickness
t = substrate thickness
σ = film stress.

Equation (1) has been derived[1,2] for the following case: The substrate is a plate that is thin, elastically isotropic, and (when bare) flat. The single film has uniform thickness, much less than t, and a uniform, isotropic plane stress. The temperature is uniform. The maximum deflection due to bending is less than about $t/2$. The composite plate (substrate plus film) is mechanically free.

The films present in integrated circuit structures have irregular geometries that complicate the understanding of mechanical behavior. In particular, it is necessary to have an understanding of the stresses that exist in these structures. Here we report the results of a comprehensive study of the stresses in interconnect lines bonded to substrates. The results are presented in a form that should permit them to be used for a wide variety of thin film stress problems.

Hence, by measuring the radius of curvature of a film/substrate composite (e.g., by an optical lever technique), film stress can, in principle, be calculated.

In practice, however, conditions arise that completely invalidate Eq. (1), require it to be modified somewhat, or simply call its accuracy into question, pending further analysis. For example, if the substrate is initially not quite flat, or if it is subjected to small, reproducible deformations other than that caused by the film stress, Eq. (1) may apply only after the non-film-stress effects are subtracted out, e.g., by making a reference measurement of the bare-substrate surface profile.[3] Also, thick-film and multiple-film cases are covered by extensions to Eq. (1) that have already been derived.[4,5] In this report, I examine (mostly theoretically) some of the effects of gravity, substrate shape, film nonuniformity, substrate crystallinity, and temperature gradients on substrate curvature.

2. Geometric Conventions, Definitions, and Basic Formulas

Geometric conventions for the composite plate as defined in Fig. 1 are adopted. Radial symmetry about the z axis is assumed unless otherwise indicated.

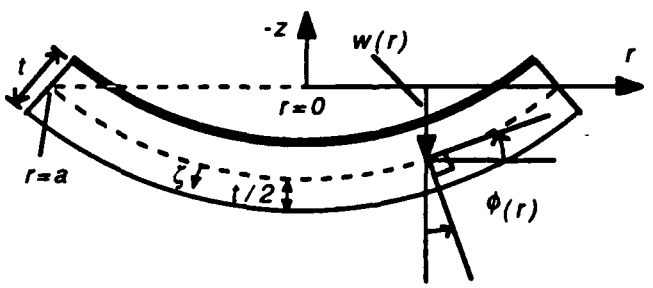

FIG. 1. Geometry (exaggerated, diametral cross section) of a bent, circular plate with film. a = radius, r = radial position, w = deflection, ζ = level, and ϕ = slope. Not shown are the cylindrical coordinate θ and Cartesian x and y axes.

The radial slope of the deflection surface is given by

$$\phi(r) = -\frac{dw}{dr}. \tag{2}$$

For small deflections, the local curvature is

$$C(r) = \frac{d\phi}{dr} = -\frac{d^2w}{dr^2} \tag{3}$$

(shown positive in Fig. 1).
If, in addition, C is constant over r, then

$$\phi(r) = \int_0^r C(r)\,dr = Cr \tag{4}$$

and

$$w_{max} = \frac{1}{2}a^2C. \tag{5}$$

The substrate, unless otherwise noted, is considered to be a *thin plate* subjected to *small deflections,* as defined below (from Ref. 6):

> In the theory of thin plates, it is customary to make the following assumptions: (1) The plate is initially flat. (2) The material is elastic, homogeneous, and isotropic. (3) Thickness is small compared to area dimensions. (4) Slope of the deflection surface is small compared to unity. (5) Deformation is such that straight lines initially normal to the middle surface remain straight and normal to that surface. (Vertical shear strains are neglected.) (6) Strains in the middle surface, arising from the deflection, are neglected compared to strains due to bending. (7) Deflection of the plate occurs by virtue of displacement of points in the mid-surface normal to its initial plane. (8) Direct stress normal to the middle surface is neglected. (9) Near edges and boundaries of loaded areas, stress resultants rather than detailed stress patterns are considered.

The flexural rigidity of the plate is defined as

$$H = \frac{Et^3}{12(1-\nu^2)}. \tag{6}$$

The biaxial modulus is

$$B = \frac{E}{1 - \nu}. \qquad (7)$$

The state of stress at a point is called equi-biaxial if there exists a Cartesian coordinate system for which two of the normal stress components are equal, the third is zero, and all shear stress components are zero; there is simply an isotropic stress acting in one plane. In this report, *biaxial stress* will refer to this isotropic stress when it is acting within, and uniform over, a given surface. The film is assumed to have biaxial stress acting parallel to the substrate surface and having an average value σ through the film thickness.

The effect of the film on the composite-plate thickness and rigidity is negligible since $h << t$ will always be assumed. The film stress is positive when tensile, negative when compressive. Bending moments per unit length, M, are positive if they tend to cause positive curvature in their plane of action.

3. Effect of Gravity

In real situations, the sample is not free, but is typically supported from below and subjected to the downward pull of gravity. The manner in which this uniform force affects the curvature depends on the position of the support points. If the support points are reproducible, as they are in a tripod arrangement of pins, then the effect of gravity on a given sample is constant and can be subtracted out by making a bare-substrate measurement. If, however, the sample sits on a flat surface (sometimes a tripod support is impractical), the support points will depend on the sample's warp. In this case, it is desirable to have an estimate of the maximum change in curvature associated with a change in support points.

Take as two extremes a horizontal, round plate (1) simply supported from below all around its perimeter and (2) supported only at its center. With q defined as the uniform downward force per area, the deflection of the plate for the edge-supported case is given by[6]

$$w_{g,\,edge} = \frac{qa^2}{64H}\left(1 - \frac{r^2}{a^2}\right)\left(\frac{5 + \nu}{1 + \nu} - \frac{r^2}{a^2}\right). \tag{8}$$

The deflection for the center-supported case can be calculated by superimposing the solutions to two different loading situations, as shown in Figure 2.

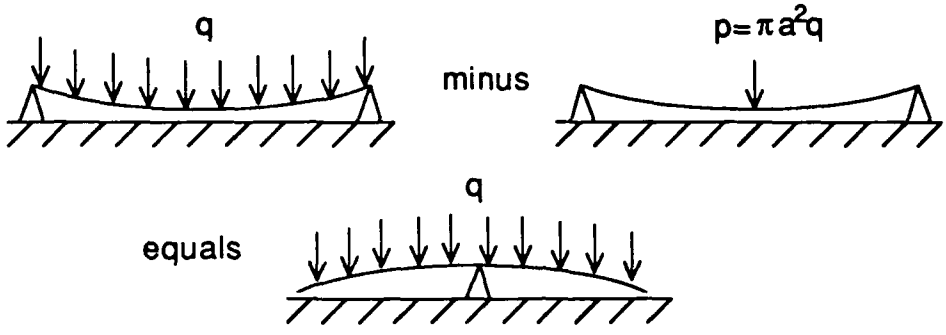

FIG. 2. Demonstration of the way in which the center-supported elastic plate-bending case is derived from the superposition of two other cases.

The result is

$$w_{g,\,center} = w_{g,\,edge} - \frac{qa^4}{16H}\left[2\frac{r^2}{a^2}\ln\left(\frac{r}{a}\right) + \frac{3 + \nu}{1 + \nu}\left(1 - \frac{r^2}{a^2}\right)\right]. \tag{9}$$

The difference between the edge and center cases is

$$\Delta w_g = w_{g,\,edge} - w_{g,\,center} = \frac{qa^4}{16H}\left[2\frac{r^2}{a^2}\ln\left(\frac{r}{a}\right) + \frac{3 + \nu}{1 + \nu}\left(1 - \frac{r^2}{a^2}\right)\right]. \tag{10}$$

The corresponding local slope and curvature, after substituting $q = \rho g t$, where ρ is the substrate mass density and g is gravitational acceleration, are

$$\Delta\phi_g(r) = -\frac{d(\Delta w_g)}{dr}$$
$$= \frac{\rho g t a^2 r}{4H}\left[\frac{1}{1+\nu} - \ln\left(\frac{r}{a}\right)\right]$$
$$= \frac{3\rho g a^2 r}{Bt^2}\left[1-(1+\nu)\ln\left(\frac{r}{a}\right)\right], \qquad (11)$$

$$\Delta C_g(r) = -\frac{d^2(\Delta w_g)}{dr^2}$$
$$= -\frac{\rho g t a^2}{4H}\left[\frac{\nu}{1+\nu} + \ln\left(\frac{r}{a}\right)\right]$$
$$= -\frac{3\rho g a^2}{Bt^2}\left[\nu + (1+\nu)\ln\left(\frac{r}{a}\right)\right]. \qquad (12)$$

(The mathematical singularity at $r = 0$ makes Eq. (12) physically unrealistic very near the center.)

The average of ΔC_g from $r = 0$ to $r = r$ on the wafer is

$$\overline{\Delta C_g}(r) = \frac{1}{r}\int_0^r \Delta C_g(r)\, dr$$
$$= \frac{1}{r}\left[\Delta\phi_g(r) - \Delta\phi_g(r \to 0)\right]$$
$$= \frac{3\rho g a^2}{Bt^2}\left[1-(1+\nu)\ln\left(\frac{r}{a}\right)\right]. \qquad (13a)$$

For the whole radius (or diameter, due to symmetry), this average reduces to

$$\overline{\Delta C_g}(a) = \left(\frac{3\rho g a^2}{Bt^2}\right). \qquad (13b)$$

Typically, however, what curvature measurement techniques actually record is an average curvature that is calculated as the slope of a linear regression best-fit line for a series of measured substrate-surface slope *vs.* diametral-position data points. If the curvature is not constant, then the measured curvature, C_m, will not in general equal the true average [as used in Eq. (13a)] of C from 0 to r,

$\overline{C}(r)$. The theoretical value of C_m can be derived from $C(r)$. Taking $C(r)$ to be the gravity effect ($\Delta C_g(r)$) given by Eq. (12) and using ten slope measurements equally spaced on a wafer diameter to calculate the measured effect, $\Delta C_{g,m}$, one can derive that

$$\Delta C_{g,m} / \overline{\Delta C_g}(a) = 1.237 + 0.237\nu \ , \tag{14}$$

which equals 1.27 for a quartz substrate ($\nu = .16$) and has a maximum possible value of 1.36 (when $\nu = .5$). The ratio $C_{g,m}/\overline{\Delta C}_g(r)$ is closer to 1 for measurements spanning less than the full diameter (i.e. $r < a$). We will subsequently to refer to the gravity effect in terms of $\overline{\Delta C}_g(a)$, keeping in mind that the magnitude of the effect as actually measured would be comparable.

In determining the film stress, we may view the maximum gravity effect as a component of the experimental uncertainty. With C_0 defined as the curvature due to film stress alone, as given by Eq. (1), then

$$\frac{\overline{\Delta C_g}(a)}{C_0} = \frac{\rho g a^2}{2\sigma h} . \tag{15}$$

Note that this *relative* variation is independent of substrate thickness and elastic moduli, but is a strong function of diameter. To reduce the relative gravity effect, one can simply use smaller substrates.

Take the example of a silicon ($\rho g = 2.33$ g/cm^3 $\times$ 980.7 dyne/gram-force) substrate with a typical film having $\sigma = 200$ MPa $= 2\times10^9$ dyne/cm^2 and $h = .5$ μm $= 5\times10^{-5}$ cm. If the substrate is a 100-mm wafer ($a = 5$ cm), then Eq. (15) gives a relative uncertainty of 29%. But $a = 1$ cm yields a very tolerable uncertainty of 1.1%. For a substrate of quartz ($\rho = 2.2$ g/cm^3, $B = 8.6\times10^{11}$ dyne/cm^2, $\nu = .16$),[7] the relative gravity effect is slightly less than it is for silicon, although the absolute effect is larger.

Experimental confirmation of the gravity effect theory is shown in Fig. 3. In this case, what is plotted is $-d(\Delta w_g)/dx$ *vs.* x, where x is the diametral position,

with the center of the substrate being at $x = 0$. The appropriate theoretical equation, a modification of Eq. (11), is

$$-\frac{d(\Delta w_0)}{dx}(x) = \frac{3\rho g a^2}{Bt^2}\left[1-(1+\nu)\ln\left|\frac{x}{a}\right|\right]. \tag{16}$$

Experimentally, slope *vs.* position data for a round quartz substrate were obtained using a laser reflection technique. The slopes that were measured while the substrate was supported at its center by a 2-mm square were subtracted (for each position) from the slopes measured when the substrate was supported around its edge by a foam ring. The resulting experimental values fit the theoretical curve quite well.

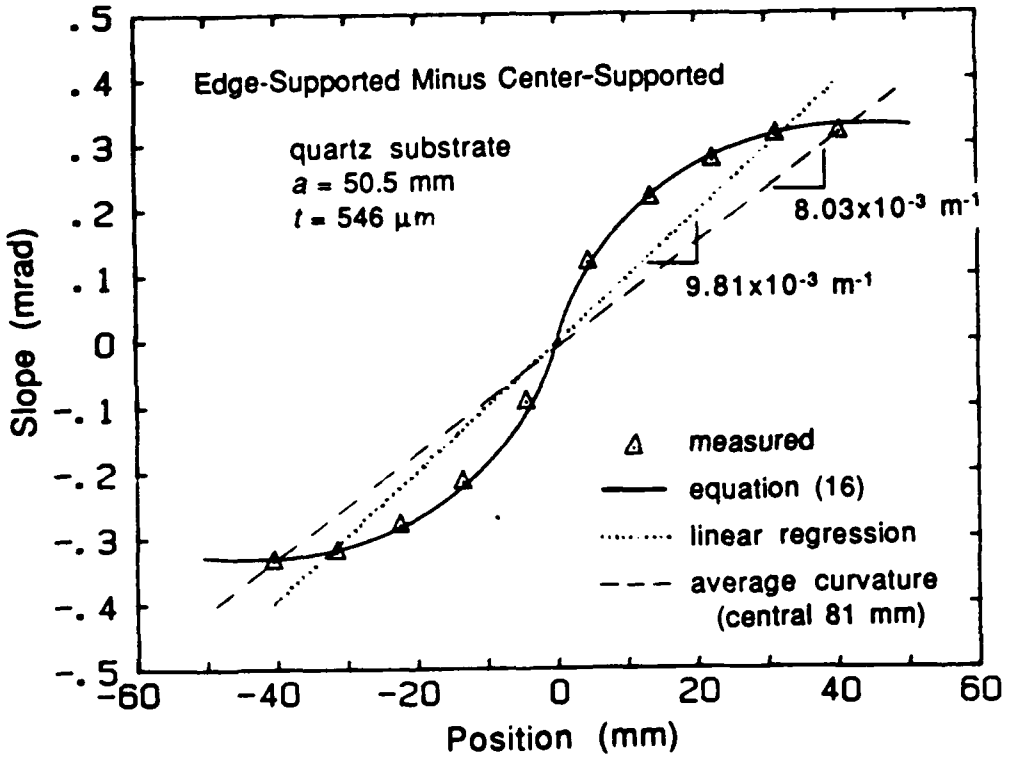

FIG. 3. Experimental confirmation of the gravity effect on a quartz substrate.

It should be noted, however, that plate deflection is very sensitive to the boundary conditions, and that in this case, a uniform, simple edge support was

hard to achieve. This difficulty resulted in some measurements varying as much as 30% from those shown. In fact, in an experiment in which the edge of the substrate was *intentionally* supported at only two points, on the line of measurement, the edge-minus-center measured curvature was 2.17×10^{-2} m^{-1}, or 2.2 times what it was with the uniform edge support. Hence the "two extremes" of support for which the equations of this section have been derived do not represent the farthest extremes of gravitational bending of an elastically-isotropic, round substrate (to say nothing of an anisotropic or rectangular one). Nevertheless, our analysis explains the general magnitude of the gravity effect and shows how it varies with substrate material and size. Such knowledge can be useful in the design of experiments and the interpretation of their results. Unless a tripod support or small substrates are used, the gravity effect is likely to be a significant source of error in determinations of film stress based on substrate curvature measurement.

4. Effect of Shape

Many researchers doing experiments that employ Eq. (1) use round substrates. But the substrate does not need to be round for Eq. (1) to hold, as the simple derivation presented here will demonstrate.

A circular plate with a uniform bending moment per unit length M applied at its perimeter deforms into a spherical cap having a curvature

$$C = \frac{M}{H(1+\nu)} = \frac{12M}{Bt^3} \qquad (17)$$

and an internal bending moment isotropically and uniformly equal to M.[6] Hence, a plate of *any* shape will deform in accordance with Eq. (17) if M is applied to its edges, since the same boundary conditions are applied to any internal section of the circular plate.

In a "strength of materials" analysis (employing Saint-Venant's principle) of the effect that a thin, stressed film has on a substrate, a force (F) and bending moment (M) per unit length acting on the perimeter of the substrate are found

that make the resultant force and moment at the edge of the film plus substrate equal zero, as illustrated in Fig. 4. The bending moment per unit length is approximately

$$M = \frac{1}{2} t\sigma h \equiv M_0. \tag{18}$$

The force per length $F_0 = -\sigma h$ acting at mid-plane does not affect the substrate curvature. Substitution of Eq. (18) into Eq. (17) yields Eq. (1). Thus, under conditions in which Eq. (1) holds for a round substrate, it also holds for a substrate plate of any other shape.

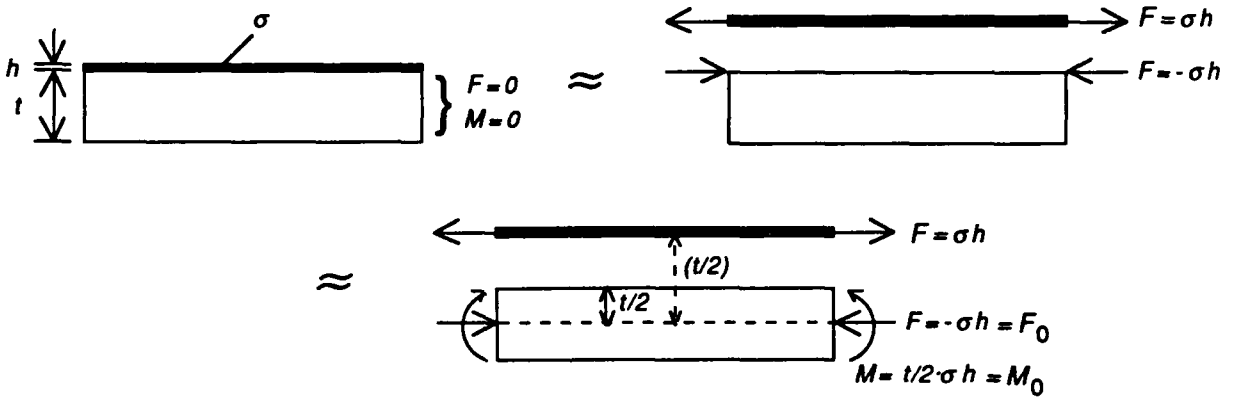

FIG. 4. Model of how a thin film exerts the approximate equivalent of a bending moment per unit length M_0 on the edge of a substrate.

However, the substrate must not be narrower than about $4t$, or it will cease to bend like a plate.[8] If the width is about equal to t or smaller, beam theory applies and $Et^3/12$ replaces H (e.g., in Eq. (17)).

Although the film effect on plate curvature is independent of the shape of the plate, the gravity effect is not; therefore, in experiments in which the gravity effect is intended to be subtracted out, the substate shape should be the same for primary and reference measurements.

5. Effect of Nonuniform Film Thickness

Thin films are sometimes not of uniform thickness over the whole area of the substrate. One way to determine the stress in such films is to cut out and measure the curvature of a section of the sample on which the film is approximately uniform. An alternative approach that involves using appropriate averages of curvature and film thickness is applicable in some cases. This method is explained below.

If, as illustrated in Fig. 5, a radial bending moment per unit length M is applied to an elastically-isotropic circular plate at $r = r_*$, then for $r \geq r_*$, the slope is[8]

$$\phi(r) = \frac{M r}{2H}\left\{\left[1 + \frac{1-\nu}{1+\nu}\left(\frac{r_*}{a}\right)^2\right] - \left[1 - \left(\frac{r_*}{r}\right)^2\right]\right\} . \qquad (19a)$$

For $r \leq r_*$,

$$\phi(r) = \frac{M r}{H(1+\nu)}\left\{1 - \frac{1-\nu}{2}\left[1 - \left(\frac{r_*}{a}\right)^2\right]\right\} . \qquad (19b)$$

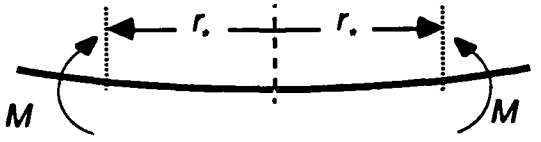

FIG. 5. Radial bending moment per length M applied uniformly to a circular plate at $r = r_*$.

In the previous section, we saw how a uniform thin film bends a substrate as if a force per unit length σh were applied to the surface of the substrate at its edge, causing an edge-applied moment $M = t\sigma h/2$. Similarly, a circular film of thickness h but extending only to $r = r_*$ on a larger substrate ($a > r_*$) would apply $M = t\sigma h/2$, but at r_* (the film's edge) instead of at the substrate's edge. Now the *applied* moment is not the same as the *internal* moment, even at r_*, since reactive moments are introduced. But the applied moment is the correct quantity to use as M in Eqs. (19a) and (19b).

A film having a radially-symmetric (with respect to a round substrate) thickness distribution *h(r)* can be thought of as the superposition of an infinite number of disks of infinitesimal (positive or negative) thickness d*h(r)*. In analogy with the macroscopic case, each of these disks exerts on the substrate a bending moment equal to

$$\mathrm{d}M(r_*) = \frac{t\sigma}{2}\mathrm{d}h(r_*)\,, \tag{20}$$

r_* being the location of the disk edge and moment application. We can imagine building the film up sequentially, starting with a disk of radius *a* and thickness *h(a)*, then adding progressively smaller disks of thickness

$$\mathrm{d}h(r_*) = \frac{\mathrm{d}h}{\mathrm{d}r_*}\mathrm{d}r_* \quad (\mathrm{d}r_* < 0)\,. \tag{21}$$

The total combined effect of these films on the slope at the edge of the substrate is

$$\begin{aligned}\phi(a) = {} & \phi(r = a,\ r_* = a,\ M = t\sigma h(a)/2) \\ & + \int_{r_* = a}^{r_* = 0} \phi(r = a,\ r_* = r_*,\ M = \mathrm{d}M(r_*))\,,\end{aligned} \tag{22}$$

where the ϕ components (here more properly $\Delta\phi$ and $\mathrm{d}\phi$) are calculated using Eq. (19a). Making the indicated substitutions yields

$$\begin{aligned}\phi(a) = {} & \frac{t\sigma h(a)a}{4H}\left\{\left[1 + \frac{1-\nu}{1+\nu}\left(\frac{a}{a}\right)^2\right] - \left[1 - \left(\frac{a}{a}\right)^2\right]\right\} \\ & + \int_a^0 \frac{t\sigma a}{4H}\,\frac{\mathrm{d}h}{\mathrm{d}r_*}\left\{\left[1 + \frac{1-\nu}{1+\nu}\left(\frac{r_*}{a}\right)^2\right] - \left[1 - \left(\frac{r_*}{a}\right)^2\right]\right\}\mathrm{d}r_* \\ & = \frac{t\sigma a}{2H(1+\nu)}\left[h(a) - \int_0^a \frac{\mathrm{d}h}{\mathrm{d}r_*}\left(\frac{r_*}{a}\right)^2 \mathrm{d}r_*\right] \\ & = \text{(using integration by parts)} \\ & \frac{t\sigma a}{2H(1+\nu)}\left[\frac{2}{a^2}\int_0^a r_* h(r_*)\,\mathrm{d}r_*\right].\end{aligned} \tag{23}$$

But

$$\frac{2}{a^2}\int_0^a r_*\,h(r_*)\,\mathrm{d}r_* = \frac{2}{a^2}\int_0^a rh(r)\,\mathrm{d}r$$
$$= \frac{1}{\pi a^2}\int_0^a 2\pi rh(r)\,\mathrm{d}r = \overline{\overline{h}}(a)\ , \tag{24}$$

where $\overline{\overline{h}}(a)$ is the average film thickness over the whole *area* of the substrate. The average curvature over a full radial or diametral *line* is

$$\bar{C}(a) = \frac{1}{a}\int_0^a C(r)\,\mathrm{d}r = \frac{1}{a}[\phi(a) - \phi(0)] = \frac{\phi(a)}{a}\ . \tag{25}$$

Combining Eqs. (23), (24), and (25) yields

$$\bar{C}(a) = \frac{t\sigma\,\overline{\overline{h}}(a)}{2H(1+\nu)} = \frac{6(1-\nu)\sigma\,\overline{\overline{h}}(a)}{Et^2}\ . \tag{26}$$

Equation (26) is the same as the uniform-film formula (Eq. (1)), but with a line-average curvature replacing C and an area-average film thickness replacing h. Rearranged, Eq. (26) can be applied to estimate σ of films that are roughly radially symmetric in thickness on a round, elastically-isotropic substrate. (If σ itself is a function of r, $\overline{\overline{\sigma h}}(a)$ is used in the equation.)

Although the complete details are not shown here, C is not constant over r when the film is not uniform. Hence, as with gravity bending, $\bar{C}(a)$, as defined by Eq. (25), is not exactly equal to the slope of a linear regression fit of ϕ *vs.* r data, except when $\phi(a)$ and $\phi(0)$ are the only points used.

It also should be noted that measuring curvature over less than the full diameter and ignoring the effect that the rest of the substrate has on that curvature can lead to erroneous calculations of stress when there is film nonuniformity. Suppose, for example, that a substrate of radius a has a film of thickness h from $r = 0$ to $r = r_*$ and is bare ($h = 0$) everywhere else. Then, with $M = t\sigma h/2$, Eq. (19b) gives the slope for $r \le r_*$ as

$$\phi(r) = \frac{6(1-\nu)\sigma h}{Et^2} r\left\{1 - \frac{1-\nu}{2}\left[1-\left(\frac{r_*}{a}\right)^2\right]\right\}, \qquad (27)$$

so the curvature for $r \le r_*$ is (using Eq. (3))

$$C(r) = \frac{6(1-\nu)\sigma h}{Et^2}\left\{1 - \frac{1-\nu}{2}\left[1-\left(\frac{r_*}{a}\right)^2\right]\right\} = C. \qquad (28)$$

Note that although the curvature is constant, in this case, over the area where the film is (it varies for $r > r_*$), its magnitude is smaller than that given by Eq.(1) by the fraction

$$Q = \frac{1-\nu}{2}\left[1-\left(\frac{r_*}{a}\right)^2\right]. \qquad (29)$$

For $\nu = .16$ (quartz) and $r_*/a = .5$, this curvature reduction is 31.5%.

FIG. 6 shows experimental verification of these equations. The bending of a 100-mm diameter barium borosilicate glass substrate ($\nu = .28$) having a 50-mm diameter circle of silicon nitride film at its center was compared to the bending of the substrate covered uniformly by the same film. The gravity effect and intrinsic substrate curviness were subtracted out of the slope *vs. x* data by means of a bare-substrate reference measurement. Equation (26) predicts that the average curvature of the nonuniform sample should be one-fourth that of the uniform sample, since its $\bar{\bar{h}}(a)$ is one-fourth as large. The experimental ratio (C_B/C_A, for a scan slightly smaller than the full diameter) is .26. Equations (28) and (29) predict that the curvature over the central 50 mm of the nonuniform sample should be constant and 27% smaller than the uniform sample's curvature. The experimental value [$(C_A-C_C)/C_A$] is 29%, with the curvature confirmed to be constant. Within experimental error, the experimental and theoretical results agree.

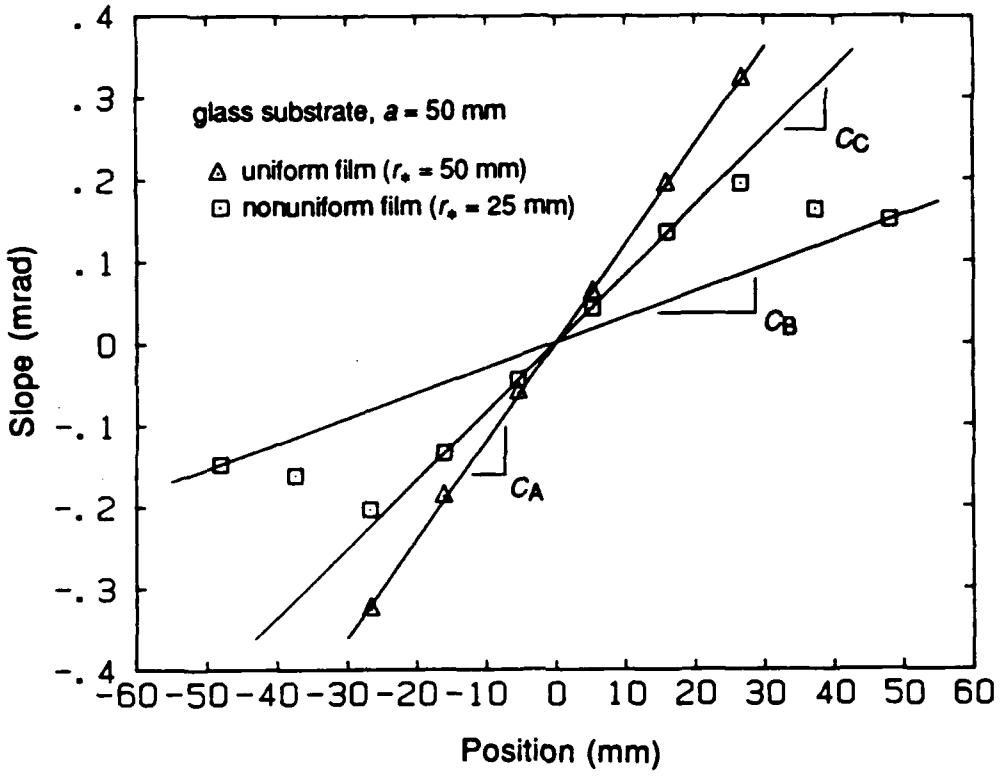

FIG. 6. Experimental measurements of nonuniform film effects. *C1* = curvature of the uniform sample, *C2* = average curvature over 96 mm of the nonuniform sample, and *C3* = curvature of central 50 mm of the nonuniform sample.

Although Eq. (26) was derived assuming radial symmetry of film and substrate, one would also expect it to apply to the case of a film that is patterned in any manner on a small scale but uniform on a large scale over a substrate of any shape. However, when film features are narrower than about 15*h*, there is a significant amount of stress relaxation in the film,[9] so the average value of σ will not be the same as the pre-patterned value.

6. Effect of Crystallinity

At the outset, I stated that the derivation of Eq. (1) includes the assumption that the substrate is elastically isotropic. Yet single-crystal substrates are often employed in thin-film stress experiments. In this section, I show that the

anisotropy associated with certain crystalline substrates is completely consistent with the bending described by Eq. (1). But for gravity bending and nonuniform-film bending, the isotropic-material equations are less applicable to the anisotropic cases.

The state of stress in an isotropic plate with a uniform applied M at its edges (as discussed in Section 4) is given by

$$\sigma_M(\zeta) = \frac{12M}{t^3}\zeta\,, \tag{30}$$

where σ_M is a biaxial stress parallel to the surface of the plate. When the bending is due to the presence of a stressed thin film, then $M = M_0$, and there is an additional biaxial stress $\sigma_{F_0} = F_0/t$ (see Fig. 4). The total biaxial stress in the substrate is then

$$\sigma_{s,0}(\zeta) = \sigma_{M_0} + \sigma_{F_0} = \frac{12M_0}{t^3}\zeta + \frac{F_0}{t} = \frac{\sigma h}{t}\left(\frac{6\zeta}{t} - 1\right), \tag{31}$$

and there are no other stresses. Since the slope of the substrate is very small, the stress state at all points in the substrate is described approximately by

$$\begin{aligned} &\sigma_1 (\equiv \sigma_x) = \sigma_2 (\equiv \sigma_y) = \sigma_{s,0} \\ &\sigma_3 (\equiv \sigma_z) = \sigma_4 (\equiv \tau_{yz}) = \sigma_5 (\equiv \tau_{xz}) = \sigma_6 (\equiv \tau_{xy}) = 0. \end{aligned} \tag{32}$$

Application of Hooke's law yields the corresponding strain state:

$$\begin{aligned} &\varepsilon_1 = \varepsilon_2 = \frac{\sigma_{s,0}}{B} = \frac{\sigma h}{Bt}\left(\frac{6\zeta}{t} - 1\right) \\ &\varepsilon_3 = -\frac{2\nu\sigma_{s,0}}{E} = -\frac{2\nu\sigma h}{Et}\left(\frac{6\zeta}{t} - 1\right) \\ &\varepsilon_4 = \varepsilon_5 = \varepsilon_6 = 0. \end{aligned} \tag{33}$$

The stress state given by Eqs. (31) and (32) is correct and unique (in the linear theory of elasticity) because[10] (1) it satisfies the equations of static equilibrium, (2) it satisfies the traction boundary conditions given[11] for all

surfaces, and (3) the strains, related to the stresses by the appropriate constitutive equation (isotropic-material Hooke's law), satisfy the equations of continuity (compatibility).[12]

The generalized form of Hooke's law for elastic anisotropic media is[13]

$$\varepsilon_i = s_{ij}\sigma_j \qquad (i, j = 1, 2, \ldots 6), \tag{34}$$

in which the s_{ij} ($= s_{ji}$) are the elastic compliances of the material. In using this equation, we shall assume that the x and y axes are parallel to the plate at an otherwise arbitrary initial orientation with respect to elastic symmetry elements in the plate.

The state of stress in an anisotropic substrate bent by a film is identical to that given [Eq. (31)] for an isotropic substrate because this state again satisfies the conditions required for a unique solution. The boundary conditions and equilibrium equations are the same as in the isotropic case, so they are satisfied. The equations of continuity, which equate sums of second derivatives of strain with respect to position, are satisfied because the strain components are simply linear combinations [by Eq. (34)] of the stress components, which vary linearly with position[14] (making all second derivatives zero).

The state of strain in the anisotropic plate remains to be determined. Substituting the stresses from Eq. (32) into Eq. (34) yields, for $i = 1$ and 2,

$$\begin{aligned} \varepsilon_1 &= (s_{11} + s_{12})\sigma_{s,0} \\ \varepsilon_2 &= (s_{12} + s_{22})\sigma_{s,0}. \end{aligned} \tag{35}$$

Converting the compliances to engineering elastic constants,[15]

$$\begin{aligned} s_{11} + s_{12} &= s_{11}\left(1 + \frac{s_{12}}{s_{11}}\right) = \frac{1}{E_{11}}(1 - \nu_{12}) \equiv \frac{1}{B_{12}} \\ s_{12} + s_{22} &= s_{22}\left(1 + \frac{s_{12}}{s_{22}}\right) = \frac{1}{E_{22}}(1 - \nu_{21}) \equiv \frac{1}{B_{21}}. \end{aligned} \tag{36}$$

The rest of the strain components are

$$\begin{aligned}\varepsilon_3 &= (s_{13} + s_{23})\sigma_{s,0} \\ \varepsilon_4 &= (s_{14} + s_{24})\sigma_{s,0} \\ \varepsilon_5 &= (s_{15} + s_{25})\sigma_{s,0} \\ \varepsilon_6 &= (s_{16} + s_{26})\sigma_{s,0}.\end{aligned} \tag{37}$$

For materials that have third order or higher rotational elastic symmetry ("polysymmetry") about the z axis, the strain state is greatly simplified. For these materials, $s_{22} = s_{11}$.[16] Thus, from Eqs. (35) and (36),

$$\varepsilon_1 = \varepsilon_2 = \frac{\sigma_{s,0}}{B_{12}}. \tag{38}$$

Also, $s_{23} = s_{13}$, so

$$\varepsilon_3 = 2s_{13}\sigma_{s,0} = -\frac{2\nu_{13}}{E_{11}}\sigma_{s,0}. \tag{39}$$

Finally, the compliances are such that

$$\varepsilon_4 = \varepsilon_5 = \varepsilon_6 = 0. \tag{40}$$

This strain state is precisely analogous to that given by Eq. (33) for an isotropic substrate, with B_{12} replacing B and s_{13} replacing $-\nu/E$. ε_1 and $\sigma_{s,0}$ are constant for rotations of the coordinate system about the z axis, hence Eq. (38) implies that B_{12} is similarly invariant. (s_{13} is invariant for z-axis rotations for *all* materials.) Thus, for substrates having z-axis polysymmetry, the curvature of any constant-ζ surface is uniform and given by an analogue of Eq. (1), specifically

$$C = \frac{6\sigma h}{B_{12} t^2}, \tag{41}$$

where B_{12} is the in-plane biaxial modulus of the plate. Values of B_{12} for four cubic semiconductor crystals in (100) and (111) wafer orientations are given in Ref. 17.

The deflection of a simply-supported anisotropic circular plate subjected to loading normal to its surface is extremely difficult to solve analytically.[18] Hence, I do not know the precise effect of crystal anisotropy on gravity bending. Certainly, Eq. (12) cannot describe the deflection of (100)-Si (fourth-order symmetric) since the equation contains ν separate from B, and the in-plane ν (ν_{12}) varies with θ for this substrate.[17] Even for (111)-Si (third-order symmetric), which has isotropic in-plane E and ν (also s_{11} and s_{12}), a radially-symmetric deflection is doubtful because shear stresses of the type σ_5 exist and s_{15} varies with θ. Nevertheless, for the purpose of estimating the magnitude of experimental uncertainty due to the gravity effect, the equations of Section 3 (perhaps using directionally-averaged elastic moduli) should be adequate for most substrate materials.

The nonuniform-film deflection equations presented in Section 5 also fail to take into account the anisotropy of (100)-Si ν_{12}. But they are probably nearly exact for (111)-Si, since, unlike the case of gravity loading mentioned above, only σ_1 and σ_2 are nonzero (at least for an isotropic substrate).

7. Effect of Thermal Gradient

In some experiments, a film on a substrate is heated while the curvature is being measured in order to determine the effect of temperature changes and annealing on film stress. Thermal gradients may exist in the substrate, and their effect on the curvature must be considered.

We will examine the case in which the substrate has a temperature that varies linearly from T at the top surface to $T + \Delta T$ at the bottom surface. This vertical thermal gradient contributes directly to curvature, since the thermal strain varies linearly with ζ. The thermally-induced curvature, which is uniform over r, is[21]

$$C_{th} = \frac{\alpha \Delta T}{t}, \tag{42}$$

where α is the thermal expansion coefficient of the substrate.

In the following examples, we will use the material parameters given in Table 1.[19,20]

Table 1

	Thermal Exp. Coef. (10^{-6} °C^{-1})		Thermal Conductivity (W/m°C)	
	α, 25 °C	α, 700 °C	λ, 300 °C	λ, 700 °C
Silicon	2.6	4.4	136	32
Fused Quartz	.50	.39	1.7	2.7

Suppose we wish to know what ΔT would cause a C_{th} of 1×10^{-3} m^{-1}, which is a small but significant curvature change, in a .5 mm-thick substrate. From Eq. (42), $\Delta T = C_{th}t/\alpha$ =

for silicon: .19 C° at 25 °C , .114 C° at 700 °C;

for quartz: 1.0 C° at 25 °C , 1.28 C° at 700 °C.

Let us calculate how much power must pass vertically through a round 100-mm wafer to cause the above effects.

$$\text{Heat flow rate} = \lambda A \frac{\Delta T}{\Delta x}; \tag{43}$$

$A = \pi(.05\text{ m})^2$, $\Delta x = t = 5\times10^{-4}$ m. The required power is

for silicon: 406 watts at 25 °C, 57 watts at 700 °C;

for quartz: 27 watts at 25 °C, 54 watts at 700 ° C

Hence, for silicon substrates at high temperatures and quartz substrates at all temperatures, vertical thermal gradients within the substrate will have a significant effect on curvature unless the furnace used has a low vertical heat flux within the compartment holding the substrate.

Horizontal thermal gradients may also exist in the substrate. They induce thermal stresses that can alter the curvature of an already-curved substrate, but the analysis of this effect will not be attempted here.

8. Summary

We have seen that the standard equation relating substrate curvature to film stress is theoretically accurate under certain experimental conditions and not accurate under others. Gravitational forces can cause a large error, but one can circumvent this problem by using small substrates or reproducible supports. The shape of the substrate, as long as it is a thin plate, does not affect the curvature-stress relation. Films of nonuniform thickness are amenable to analysis by a simple analogue of the classical curvature-stress relation in certain cases. The crystallinity of (111)- or (100)-oriented cubic-material substrates, among others, necessitates another analogue. Thermal gradients can significantly alter substrate curvature. These pieces of information should be valuable to researchers measuring stresses in thin films on substrates.

1. G. G. Stoney, "The tension of metallic films deposited by electrolysis," Proc. R. Soc. London Ser. A **82**, 172-175 (1909).

2. R. W. Hoffman, "The mechanical properties of thin condensed films," in *Physics of Thin Films*, edited by G. Hass and R. E. Thun (Academic Press, New York, 1966), Vol. 3, p. 211.

3. P. A. Flinn, D. S. Gardner, and W. D. Nix, "Measurement and interpretation of stress in aluminum-based metallization as a function of thermal history," IEEE Trans. Electron Devices ED-**34**, 689-699 (1987).

4. N. N. Davidenkov, "Measurement of residual stresses in electrolytic deposits," Sov. Phys.–Solid State **2**, 2595-2598 (1961).

5. P. Townsend, D. M. Barnett, and T. A. Brunner, "Elastic relationships in layered composite media with approximation for the case of thin films on a thick substrate," J. Appl. Phys. **62**, 4438-4444 (1987).

6. S. Way, in *Handbook of Engineering Mechanics*, edited by W. Flügge (McGraw-Hill, New York, 1962), Chap. 39.

7. *CRC Handbook of Chemistry and Physics*, 59th ed., edited by R. C. Weast (CRC Press, Boca Raton, Florida, 1979), p. F-80.

8. R. J. Roark and W. C. Young, *Formulas For Stress and Strain*, 5th ed. (McGraw-Hill, New York, 1975), Chap. 10.

9. M. Murakami, T.-S. Kuan, and I. A. Blech, "Mechanical properties of thin films on substrates," *Treatise on Materials Science and Technology* (Academic Press, New York, 1982), Vol. 24, pp. 163-210.

10. P. Boresi and K. P. Chang, *Elasticity in Engineering Mechanics* (Elsevier, New York, 1987), p. 318.

11. The actual tractions are assumed to be equivalent, in their effect away from the edges, to a normal edge-traction distribution of the form given by Eq. (30).

12. However, when w_{max} approaches $t/2$, the applicability of the classical linear elasticity equations degrades to the point where Eq. (30) [and hence Eq. (1)] are substantially in error. See: S. Timoshenko, *Theory of Plates and Shells* (McGraw-Hill, New York, 1940), pp. 329-332.

13. J. F. Nye, *Physical Properties of Crystals* (Clarendon Press, Oxford, 1985), pp. 131-135.

14. Although ζ may differ significantly from z, the angle between their directions of measure is very small, so $\partial/\partial z \approx \partial/\partial\zeta$.

15. R. F. S. Hearmon, *An Introduction to Applied Anisotropic Elasticity* (Oxford University Press, London, 1961), Chap. 1.

16. S. G. Lekhnitskii, *Theory of Elasticity of an Anisotropic Elastic Body* (Holden-Day, San Francisco, 1963), Chap. 3.

17. W. A. Brantley, "Calculated elastic constants for stress problems associated with semiconductor devices," J. Appl. Phys. **44**, 534-535 (1973).

18. H. Okubo, "Bending of a thin circular plate of an aeolotropic material under uniform lateral load (supported edge)," J. Appl. Phys. **20**, 1151-1154 (1949).

19. *Thermal Expansion*, edited by Y. S. Touloukian, R. K. Kirby, R. E. Taylor, and P. D. Desai (IFI/Plenum, New York, 1977), Vol. 13.

20. *Thermophysical Properties of High Temperature Solid Materials*, edited by Y. S. Touloukian. (Macmillan, New York, 1967), Vol. 1 and Vol. 4, Part 2.

21. R. J. Roark and W. C. Young, *Formulas For Stress and Strain*, 5th ed. (McGraw-Hill, New York, 1975), p. 583.

B. Redesigned Furnace and Ambient Gas Control for Thin-Film Stress Measurement System (F. von Preissig)

1. Background

Currently, we have an apparatus that measures mechanical stress in thin-film materials on substrates. Film stress is calculated from optically-measured substrate curvature. Ours is one of the very few systems that attempt to heat the sample while measuring its stress. This permits *in-situ* monitoring of thermally-induced changes in the film material that are reflected in the changing stress. Although our system has proved to be an important research tool, its heating chamber has certain inadequacies and limitations that make it unsuitable for the new generation of experiments that should be done. I have designed and am building a new furnace that should eliminate the problems and add new capabilities. This furnace is now near completion. In addition, I have created equipment to introduce argon-diluted steam into the sample compartment.

2. Problems With the Current Furnace

The sample substrate sits directly on a flat graphite susceptor. Since the substrate is not perfectly flat, it contacts the surface discontinuously and in an unpredictable way, causing two main problems. First, the effect of gravity on curvature, which can be large, is not constant, so it cannot be subtracted out using a reference measurement. Second, the sample may shift and wobble during the experiment, adding scatter to the data, due to unstable seating.

Since heat is supplied only from below, large thermal gradients exist in the sample compartment. These temperature differences probably don't affect the sample temperature much when the substrate sits on the graphite (containing the measurement thermocouple). However, in order to counter the gravity and stability problems, the substrate would need to sit on a tripod slightly above the graphite surface. But when this is done, the sample temperature differs significantly from that measured by the thermocouple (40 C° at 400 °C). For

most studies of kinetic processes, even ten-degree errors are not tolerable. Temperature gradients are also responsible for gas-density fluctuations, which deflect the laser beam, and can induce thermal-strain curvatures in the substrate.

The sample is exposed to insulation material within the gas-tight compartment. This configuration reduces ambient gas (e.g., argon) purity.

3. Description and Capabilities of the New Design

The new furnace, shown schematically in Fig. 1, has a fused-quartz inner chamber, including a gas-tight seal. Hence, the ambient gas remains pure, and reactive gases such as oxygen and steam may be introduced.

Surrounding the quartz on all sides (leaving an optical opening) is a thermally-conductive graphite sheath, heated from above and below. This arrangement will essentially eliminate thermal gradients in the sample compartment.

The sample substrates rest on quartz tripods within the chamber, thus sustaining a constant, subtractable gravity effect and attaining seating stability. Since there are no thermal gradients, the sample temperature is accurately measured (at least in the steady state) by a thermocouple probe in the sample compartment.

The furnace opens in such a way that samples can be inserted and removed (by means of a vacuum chuck assembly) quickly while the furnace is hot (see Fig. 2). Samples will heat up to a constant annealing temperature in about a minute instead of the 10-20 minutes currently possible. Annealing temperatures up to 990 °C will be possible.

The ambient-control system shown and described in Fig. 3 complements the new furnace's capability of handling steam for use in solid-gas reaction experiments.

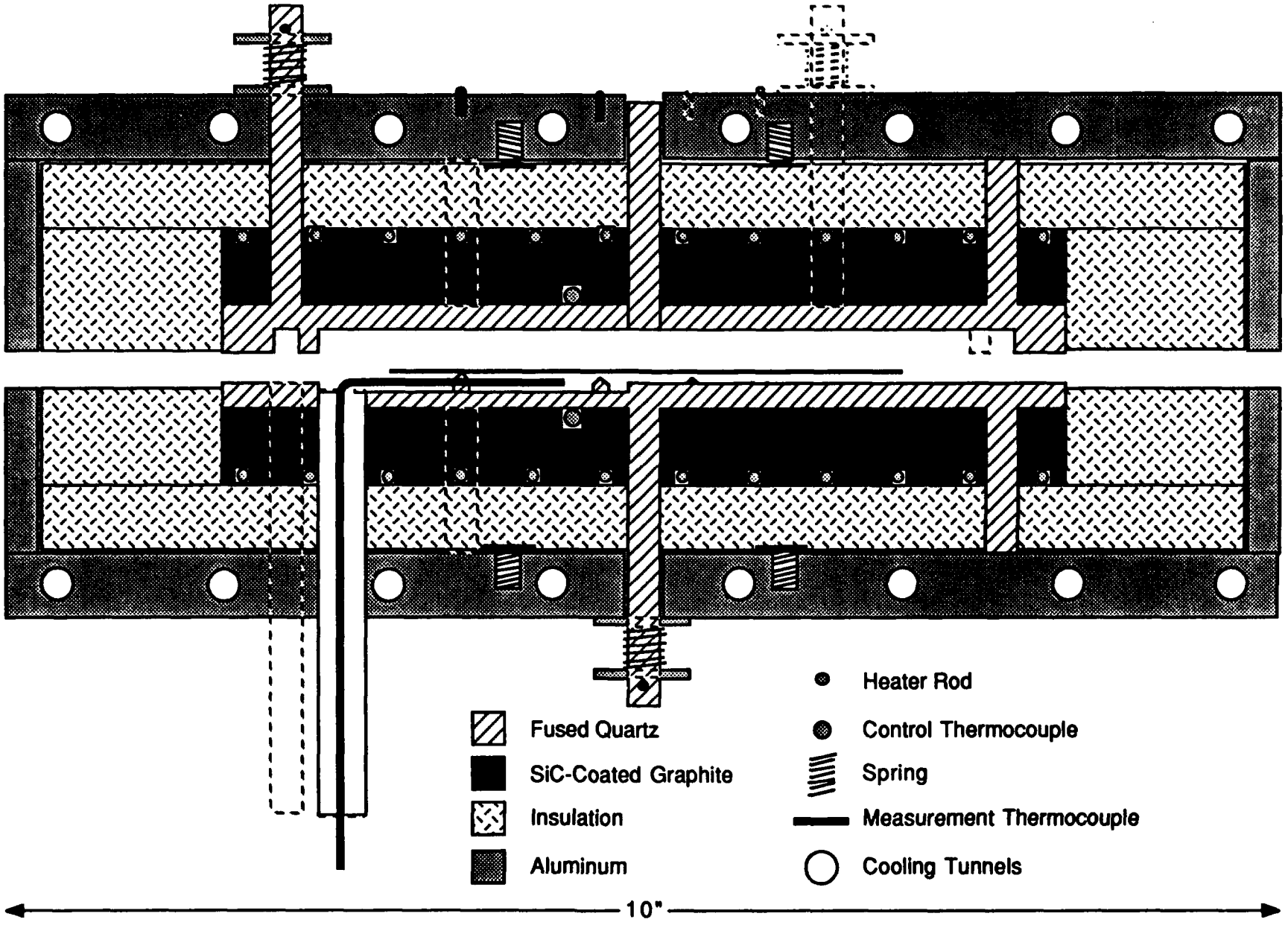

FIG. 1. Cross section of new furnace.

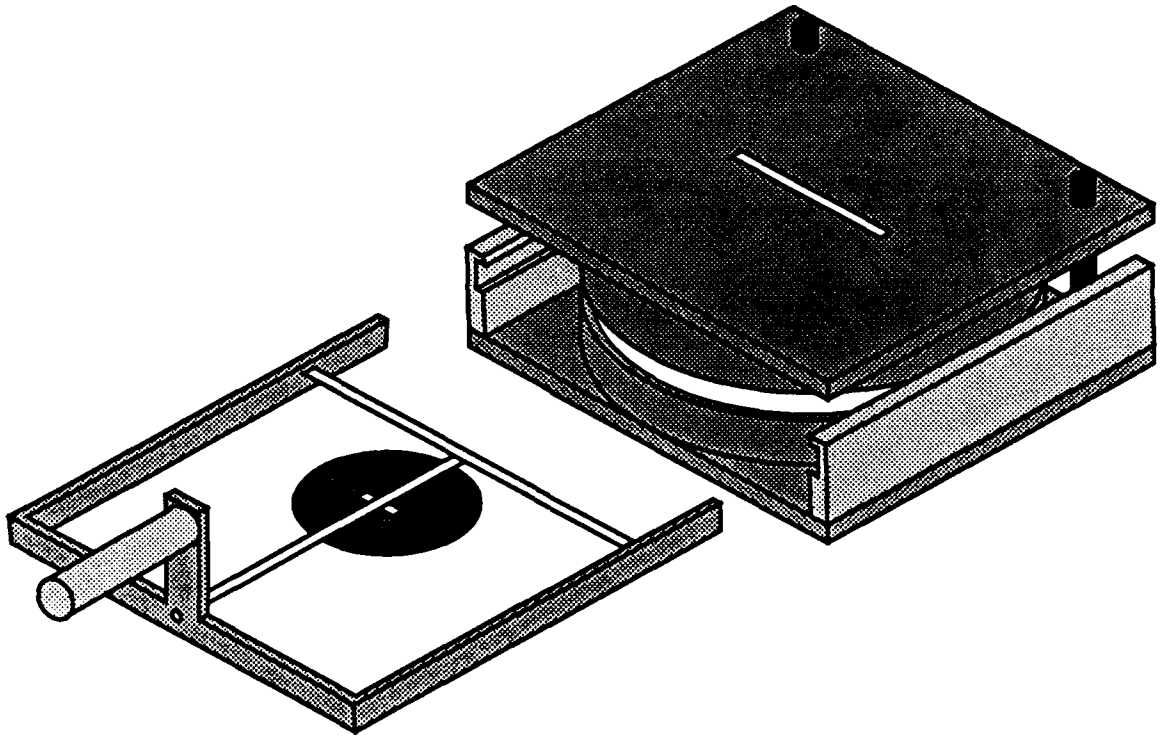

FIG. 2. Furnace ready to accept sample carried by vacuum chuck assembly.

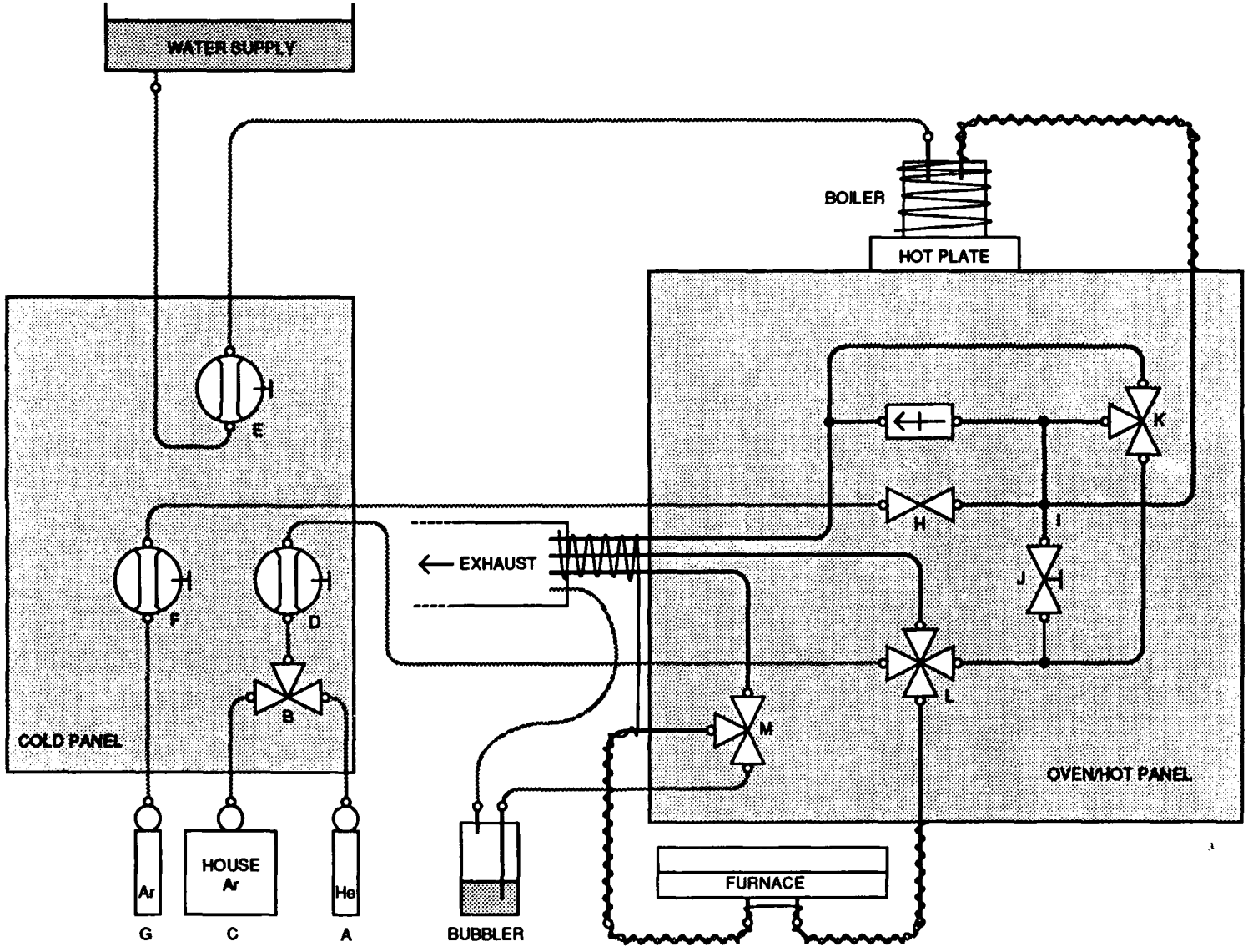

FIG. 3(a) Ambient gas control system.

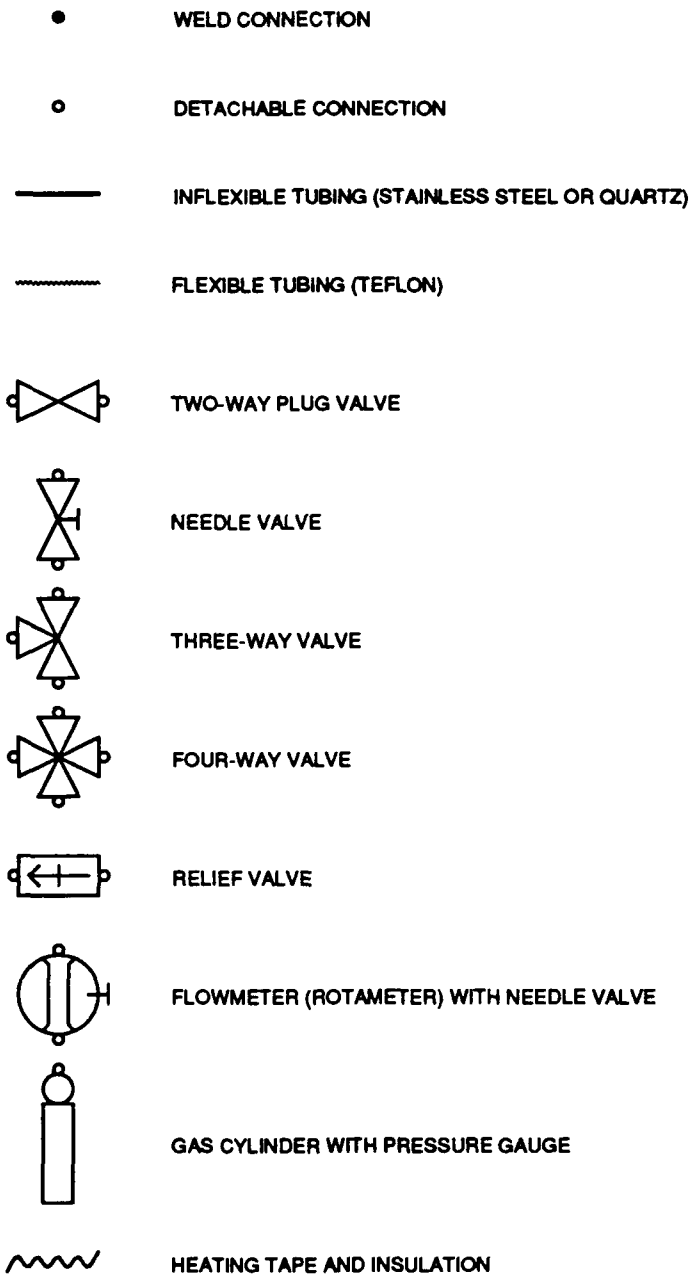

FIG. 3(b). Gas control symbols.

All-Dry Mode

For experiments requiring an inert-gas ambient, helium and argon can be used. Typically, the furnace is purged of air by helium (**A**) immediately after sample insertion. The high thermal conductivity of helium minimizes the time it takes for the sample to reach furnace temperature. After the temperature has stabilized, valve **B** is used to switch from helium to argon (**C**) flow, and argon is used for the remainder of the experiment. The inert-gas flow rate is controlled by flowmeter **D**. After leaving the furnace, inert gases percolate through silicone oil in the bubbler to eliminate back-diffusion of air into the furnace. The gas pressure in the furnace is always approximately one atmosphere.

Steam/Dry Mode

Pure steam is produced when de-ionized water from a storage tank situated above the apparatus flows through flowmeter **E** at a controlled rate and is vaporized at the same rate in the boiler. The steam can be diluted a desired amount by argon controlled by flowmeter **F**. A separate argon cylinder (**G**) is used for this purpose to prevent possible contamination of house argon by water vapor. To reduce contamination of this cylinder, a plug valve (**H**) is closed when no diluent argon is flowing. Diluent argon and pure steam mix at junction **I**. The portion of this mixed gas to be used in the long term is controlled by needle valve **J**. The rest either exits to the exhaust vent or is shunted toward the furnace for use as an initial purge, depending on the setting of valve **K**. The four-way valve (**L**) allows an instantaneous switch to be made between wet and dry gases flowing through the furnace (with the gas not currently selected going directly to the exhaust). Valve **M** is used to send dry gas through the bubbler and wet gas directly to the exhaust.

FIG. 3(c). Gas control operation.

4. Planned Experiments

Studies have begun on the following material processes: (1) Densification and flow in borophosphosilicate glass (BPSG) films upon annealing. (2) Water diffusion in BPSG films exposed to wet and dry ambients at various temperatures. (3) Crystallization in amorphous silicon films upon annealing. It may also be possible to monitor wet oxidation of silicon *in-situ*. Preliminary results indicate that the associated stress changes are large and can be used to learn about the kinetics of these processes.

C. Mechanical Properties of Thin Aluminum Metallizations

(J.F. Turlo)

As the dimensions of integrated circuits continue to shrink, an understanding of the mechanical properties of thin films becomes ever more important to device manufacture, operation and reliability. Several methods have been used to study thin film stresses. The variation of film stress with film thickness has been monitored by measuring the deflection of thin cantilever beams which act as the substrate during deposition. X - rays have frequently been used to measure the elastic strain of the substrate and this can be related to the stress in the film. Also, lasers have been used in several ways to measure sample curvature, which can also be related to the stress in the film.

At Stanford, a laser based curvature measurement system has been designed for quick and convenient acquisition of thin film stress data. A laser beam is aimed at a mirror that is mounted on a shaft whose rotation angle can be precisely controlled. The beam then travels to the sample. As the shaft rotates, the laser beam sweeps across the sample. In addition, the beam passes through a lens so that the beam will strike the sample at the same incident angle regardless of shaft angle. After reflection from the sample, the beam passes back through the lens which focuses it onto a position sensing photodiode. The sample curvature is obtained from a plot of the shaft angle versus the photodiode signal. A single curvature measurement at room temperature can be made in about 10 seconds. The system can also heat a sample to 450 °C at 0 to 10 degrees per minute.

The system has a theoretical resolution of 25×10^{-6} m^{-1}, which corresponds to a surface with a 40 kilometer radius of curvature. In practice, the system displays a resolution of 1×10^{-3} m^{-1} or a 1000 meter radius of curvature. The corresponding stress resolution is about 10 MPa but is sample dependent. The overall system accuracy is roughly 5 %. A typical curve of stress versus temperature obtained with this system is shown in Figure 1.

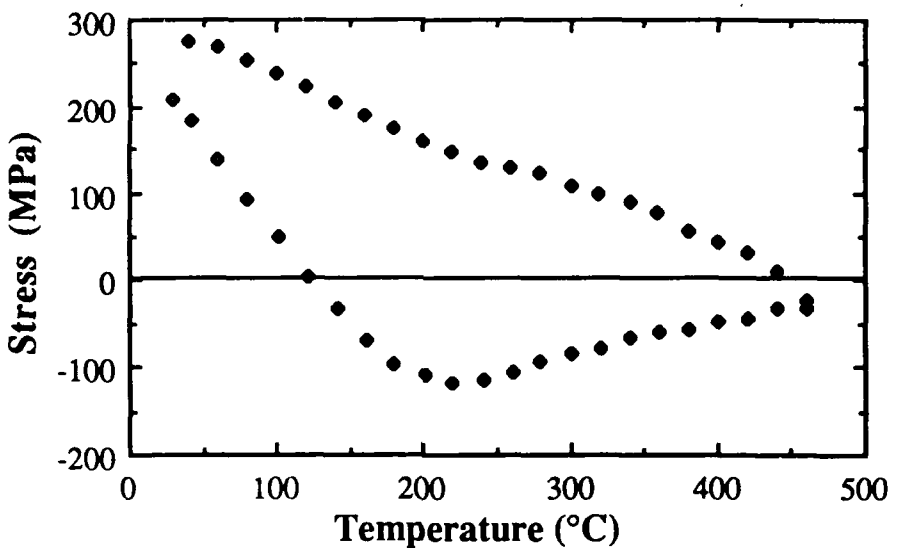

Figure 1. A typical plot of stress versus temperature for a 1 micron Al - 1% Si film on a silicon substrate. The open diamonds are heating data and the filled diamonds are cooling data.

During heating, the stress changes by elastic deformation until a temperature and compressive stress are reached that cause significant plastic flow. The maximum compressive stress attained is about 120 MPa which corresponds to about 17 ksi. Bulk aluminum samples typically yield between 5 and 15 ksi. During cooling, no notable elastic range is discernible but, the flow stress in tension increases with decreasing temperature. A change in slope is seen at about 250°C, which could be due to precipitation of silicon. The feature is more apparent in samples that contain copper.

The results in Figure 1 are complicated by the fact that stress is a function of both temperature and time. But, isothermal tests can also be performed. A typical stress relaxation curve is shown in Figure 2.

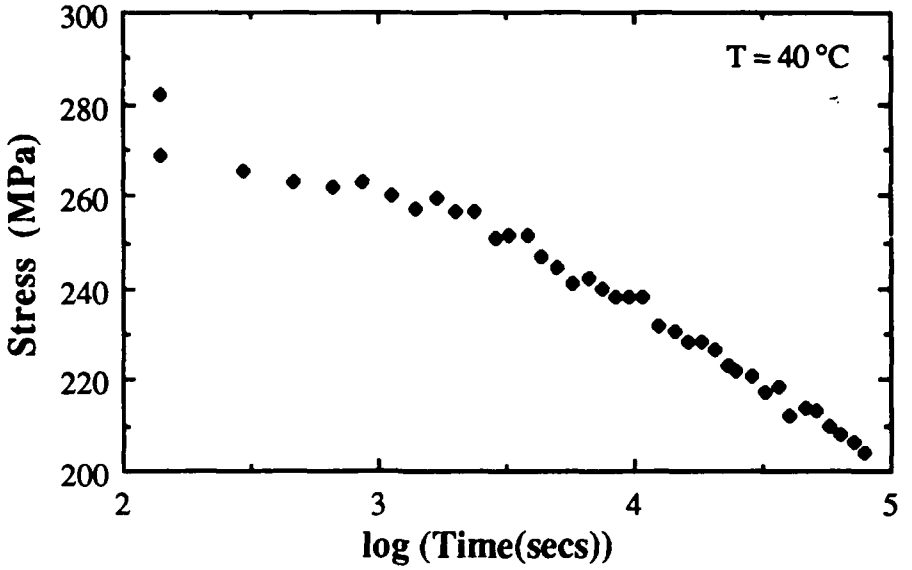

Figure 2. Stress relaxation data for a 1 micron aluminum film on a silicon substrate.

The advantage of an isothermal test is that the data can be cast into a standard rate form and compared to bulk data. In doing so for several samples, the stress at a given strain rate is seen to be higher for thin film aluminum, implying a higher resistance to plastic flow than in bulk samples. However, the data is sparse and somewhat inconsistent. In fact, the log of stress was plotted against the log of time for many isothermal tests to determine the stress exponent in the simple equation,

$$\dot{\varepsilon}_p \propto \sigma^n$$

but the resulting exponent, n, varied between 7 and 40.

The inconsistencies in the above data could be caused by the furnace which suffers severe wear and distortion during thermal cycling. At times, the temperature has been found to be inaccurate by as much as 10 %. Another part of the problem could be that the system can only accurately resolve a stress of 10 MPa. The stress in Figure 2 only varies 80 MPa in 24 hours at one third of

the melting point of aluminum while tests at higher temperatures may begin at only 50 MPa and vary by only 20 MPa. Lower temperature tests cannot be performed.

Consequently, a system has been designed and is being built that will allow a wider range of testing conditions with improved accuracy. The design specifications include heating and cooling capabilities between -50°C and 800°C at -20°C to 20°C per minute. The theoretical resolution is over 100 kilometers but, the actual resolution will be much less. The expected stress resolution is less than 1 MPa with an accuracy of better than 1 %.

Typical factors influencing the mechanical behavior of metals include composition, grain size and structure but, thin films have also shown dependence on film thickness, presence of oxides and interface quality. The stress in a 0.2 micron thick aluminum film has been found to be 600 MPa, which is five times the stress in a 1 micron thick film. And, as noted, precipitation hardening seems to play some role in film strength but the effect has not been quantified.

In an effort to obtain a greater understanding of the mechanisms governing the strength properties of aluminum thin films, a more complete study will be conducted using the new curvature measurement device. General thermal cycles, as in Figure 1, and isothermal tests, as in Figure 2, will be performed over a range of film parameters to determine the magnitude of their effect. In addition, isothermal results can be related to bulk data and established deformation mechanisms.

D. Finite Element Calculations of Thermal Stresses in an Unpassivated Line Bonded to a Rigid Substrate

(A.I. Sauter)

1. Introduction

Stresses develop in integrated circuit structures during processing and service as a result of a variety of effects. Thermal expansion coefficients of neighboring materials may be sufficiently different that temperature changes produce significant stresses. Also, adjoining materials may react in such a way that the product phases have a volume which differs from that of the reacting phases. This, too, results in the generation of stresses. In addition, stresses develop naturally in epitaxial films when their lattice parameters differ from that of the substrate. In short, there are many possible sources of stresses in integrated circuits. These stresses can lead to plastic flow, cracking, void formation, and eventually failure of the circuit. It is therefore of interest to know the magnitudes and concentrations of such stresses.

Considerable attention has been focussed on the stresses in continuous thin film layers. Stresses in thin films arising from epitaxial, thermal and growth mechanisms have been well studied and are generally understood. However, thin film materials used in integrated circuit technology are almost exclusively found not as continuous films but as patterned films. Thus it is of interest to study the stresses as they develop in irregular, patterned structures. Interconnect metals are particularly susceptible to thermal stresses, because their thermal expansion coefficients are so much greater than all of the other materials involved. The other materials are usually covalently bonded insulators and semiconductors and have similar thermal expansion coefficients, while the thermal expansion coefficients of the metals can be up to an order of magnitude larger. For example, one of the most widely used metallization materials is aluminum. Its thermal expansion coefficient is 23.6×10^{-6} / °C, while that for Si is about 4×10^{-6} / °C.

It is important to understand how stresses in patterned films differ from those in continuous films. As yet, the stresses in patterned films have not been measured or characterized in a comprehensive way. It is often difficult to

calculate the expected stresses under a given set of conditions because of the often complicated geometries involved. However, the finite element method can be used to find the thermal stresses in these cases [1].

2. The Finite Element Method

The finite element method is used in the present work to find the distribution of stress in a long line of film bonded to a rigid substrate and subjected to a thermal strain. The geometry involved and a sample mesh are shown in Figure 1. The thickness of the line is h and its width is w. Calculations have been made for width to thickness ratios of w/h = 2, 4, 6, 8, and 10. Note that the y-z plane is a plane of symmetry for the line, so the mesh only covers the right half of the line. The left half of the line is simulated by the boundary condition that there be no x displacements on the plane x = 0. Also, two dimensional plane strain elements are used in the mesh. The strain in the z direction is taken to be zero; this naturally causes σ_{zz} stresses to develop in the line.

The MARC finite element program was used to solve the problem of thermal stresses in a long thin line bonded to a rigid substrate. The meshes used were generated using the MENTAT program. The material properties of Al and a temperature change of -475°C (from 500°C to 25°C) were used in the calculation, but the results presented have been normalized to make them material and temperature difference independent. In order to test whether the meshes were fine enough to give accurate results, the element size was refined by a factor of two; the results were not significantly different. It was concluded that the original meshes were sufficiently fine to show the important features of the stress distributions in the lines. All calculations were made using a VAXstationII/GPX computer.

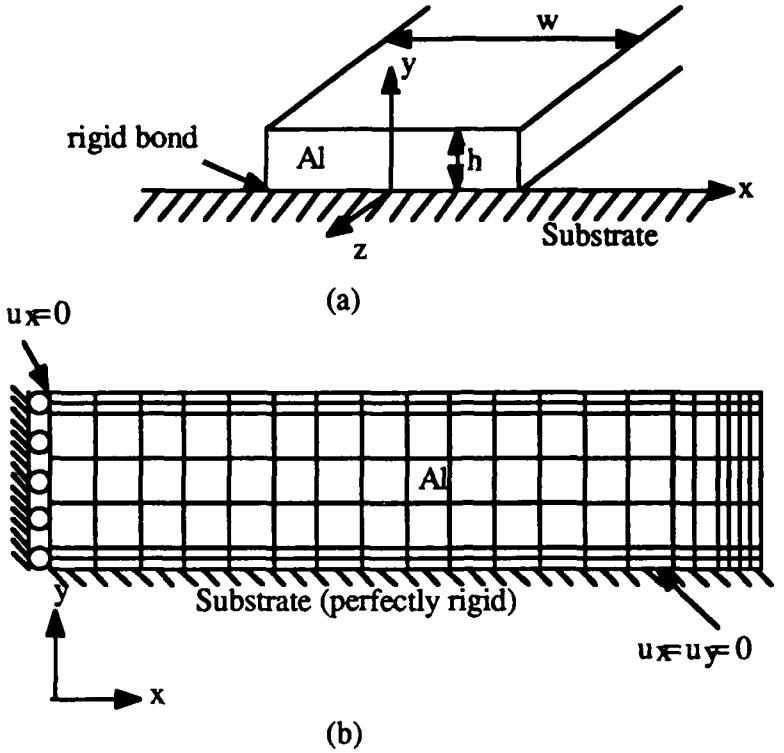

Figure 1. (a) A schematic of the geometry of the problem. The y-z plane is a plane of symmetry. (b) A sample mesh for an aspect ratio of w/h = 8. The boundary conditions are shown. Note that the left half of the line is omitted due to symmetry.

3. Plane Stress vs. Plane Strain

In 1949, Aleck [2] numerically solved the problem of thermal stresses induced in a thin rectangular plate clamped along one edge. The current problem is very similar to Aleck's problem, except that Aleck used plane stress conditions for his plate while the more suitable condition for a long thin line is plane strain. Plane stress calculations were also made in order to compare them with the previous numerical results. Figure 2 shows the distribution of transverse thermal stress, σ_{xx}, in a line with an aspect ratio of w/h = 10. The plane stress numerical results of Blech and Levi [3] obtained using Aleck's method are compared with the finite element results. Good agreement between the two methods is found. The main difference between the two is that the finite element results do not show the stress at the interface (y/h = 0) returning to zero at the edge of the line, but rather indicate a sharp increase in stress. In fact the stress calculated at that point should depend on the path used to approach the

point [4]. It should be zero, as Aleck shows, if the point is approached from outside the line, or along the outer edge of the line. However, it may have some other value if approached from inside the line, as a singularity exists there. So the discrepancy is probably due to a difference in calculation paths. Thus, except for this point, we conclude that the finite element method can give an accurate solution to this problem.

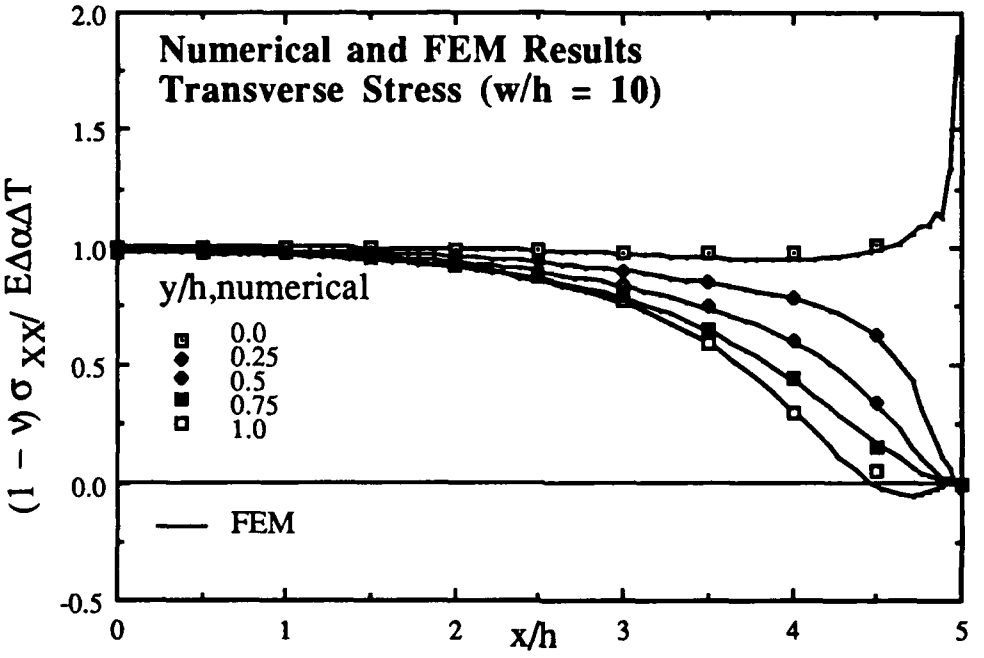

Figure 2. A comparison of numerical and FEM results for the plane stress case, showing the transverse stress in a line of w/h = 10 aspect ratio. The numerical results are those of Blech and Levi [3].

For both the plane strain and plane stress cases, the stresses are normalized by the value of σ_{xx} that would exist in the center of the line at the interface between the line and the substrate if the line were very wide. These values are computed as follows: For the case of plane stress ($\sigma_{zz} = 0$), $\sigma_{yy} = 0$ because there is no constraint in the y direction (Figure 3(a)). Since the line is perfectly bonded to the substrate,at the interface the total strain in the x direction must be zero, hence: $\varepsilon_{xx,elastic} = -\varepsilon_{xx,thermal}$. By Hooke's law,

$$\varepsilon_{xx,\,elastic} = \frac{1}{E}\left[\sigma_{xx} - \nu\left(\sigma_{yy} + \sigma_{zz}\right)\right] = \frac{\sigma_{xx}}{E} \qquad (1)$$

where E is Young's modulus of the film, and ν is Poisson's ratio. The thermal strain is given by $-\Delta\alpha\Delta T$, where $\Delta\alpha$ is the difference in thermal expansion coefficients between the film and the substrate, and ΔT is the difference between the initial and final temperatures. Thus the transverse stress at the center of a wide line is given by

$$\sigma_{xx} = E\Delta\alpha\Delta T \tag{2}$$

For the case of plain strain, $\sigma_{yy} = 0$ as before, but $\sigma_{zz} = \sigma_{xx}$, since the middle of a long wide line should behave exactly like a thin film, and therefore have a biaxial stress state (Figure 3(b)). As before,

$$\varepsilon_{xx,\,elastic} = \frac{1}{E}\left[\sigma_{xx} - \nu(\sigma_{yy} + \sigma_{zz})\right] = \frac{(1-\nu)\sigma_{xx}}{E} \tag{3}$$

so for the case of plane strain, the expected stress is given by

$$\sigma_{xx} = \frac{E}{(1-\nu)}\Delta\alpha\Delta T \tag{4}$$

Thus, it is expected that near the center of a wide line the transverse stress for plane strain will be larger than for plane stress by a factor of 1/(1-ν). This prediction is borne out by the finite element results, as for both plane strain and plane stress the normalized transverse stress approaches 1.0 at the center of the line as the line width increases. In all of the figures showing normalized stress, the normalization factor is given by equation (2) for plane stress and equation (4) for plane strain.

Aleck's results have been used by others [5,6] to describe stresses in thin film structures, however these authors left the calculation in plane stress form. Although it is possible to approximate the plane strain results by dividing the plane stress results by (1-ν), the exact form of the stresses cannot be obtained by this procedure.

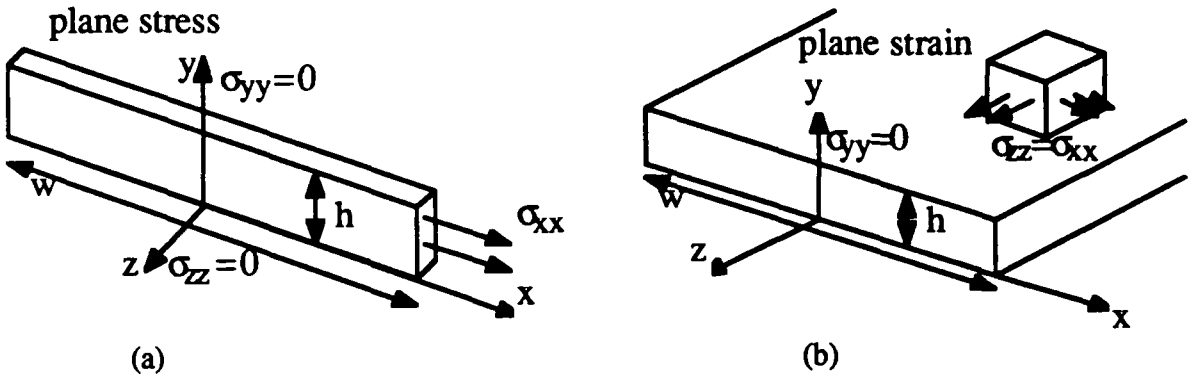

Figure 3. (a) Aleck's geometry, suitable for plane stress calculations. (b) The geometry of a line of metallization, suitable for plane strain calculations.

4. Results

The transverse, shear, normal, and longitudinal stresses (σ_{xx}, σ_{xy}, σ_{yy} and σ_{zz}) are shown for a line with aspect ratio w/h = 6 in Figure 4. They are plotted for five different values of y/h. With the mesh that was used, it was not possible to calculate the stresses at y/h = 0 and y/h=1, so the results are given for y/h = 0.00704 and y/h = 0.993 instead. Thus the stresses at the interface and at the top surface of the line are not known exactly. The transverse stress, Figure 4(a), approaches its expected value at the center of the line near the interface. The stress drops to zero at the edge of the line (x/h = 3) except near the interface, where there is a singularity.The shear stress, Figure 4(c), is zero at the top of the line, becoming larger as one approaches the interface and having a maximum at each y value near the edge. At the interface, the shear stress appears to have a singularity at the edge. Again, this may be a matter of calculation path, or it may be that there is a turn toward zero in this curve that is so near the edge it is impossible to detect with the FEM program in use. The normal stress, Figure 4(b), is very small for three-quarters of the width of the line, reaches a maximum near the edge and returns to zero, except for at the interface where there is an apparent singularity as with the other components. The longitudinal stress, Figure 4(d), is fairly constant throughout the width and height of the line, except for the sharp rise near the edge at the interface, and its value is very near the biaxial normalizing stress.

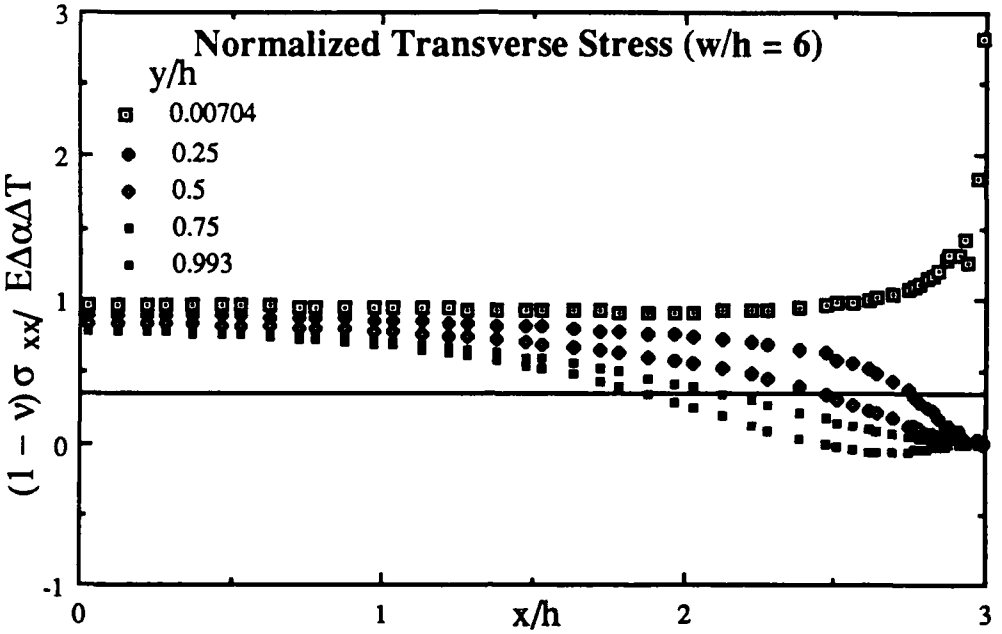

Figure 4(a) Normalized transverse stress at various y/h values for an aspect ratio of w/h=6. The normalization factor in all cases is [E/(1-ν)]ΔαΔT. All of these stresses are calculated under plane strain conditions.

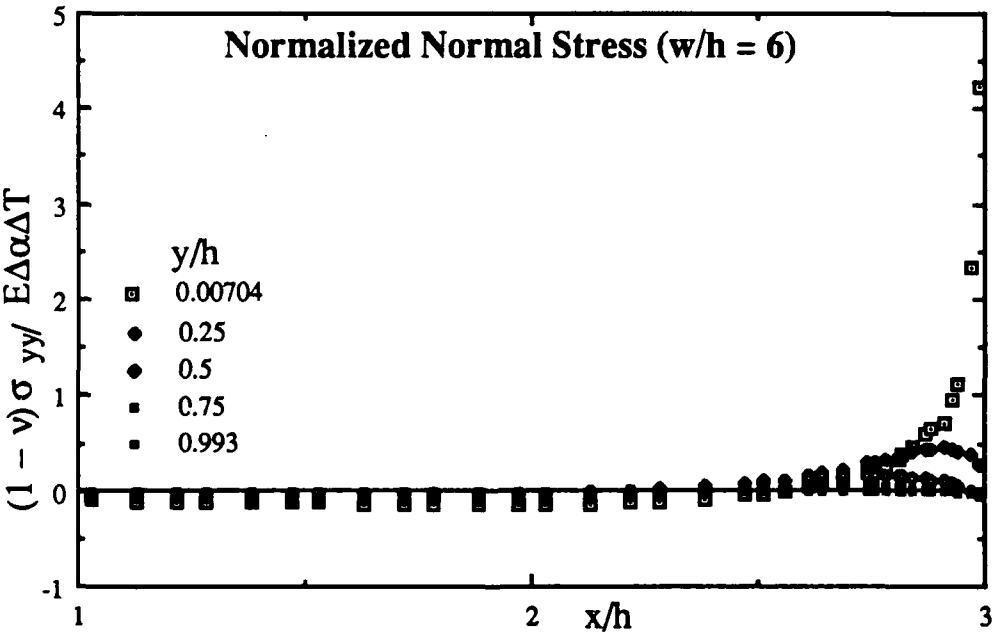

Figure 4(b) Normalized normal stress at various y/h values for an aspect ratio of w/h=6. The normalization factor in all cases is [E/(1-ν)]ΔαΔT. All of these stresses are calculated under plane strain conditions.

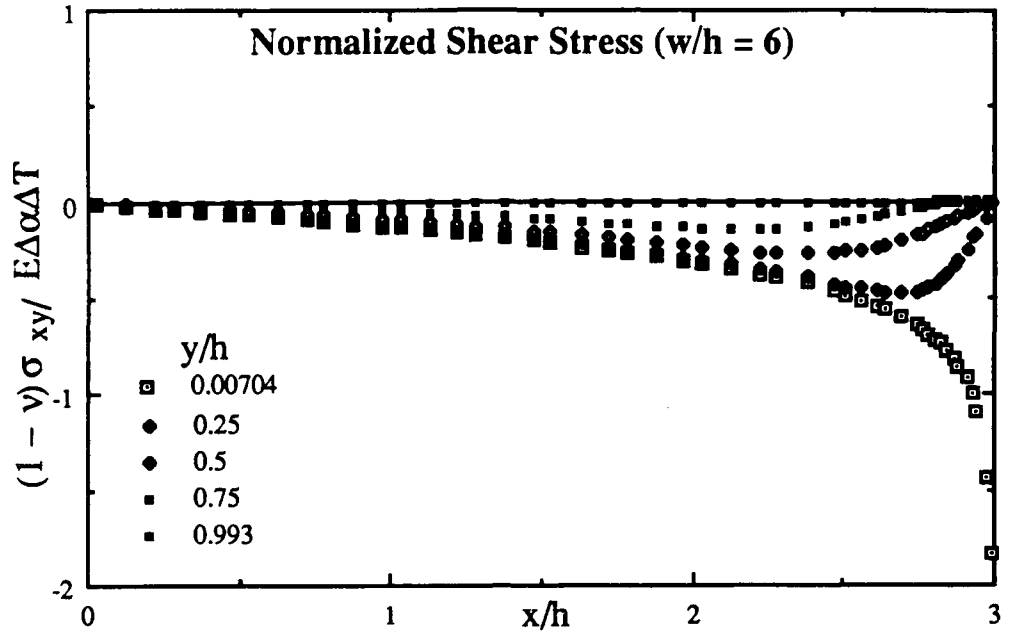

Figure 4(c) Normalized shear stress at various y/h values for an aspect ratio of w/h=6. The normalization factor in all cases is [E/(1-ν)]ΔαΔT. All of these stresses are calculated under plane strain conditions.

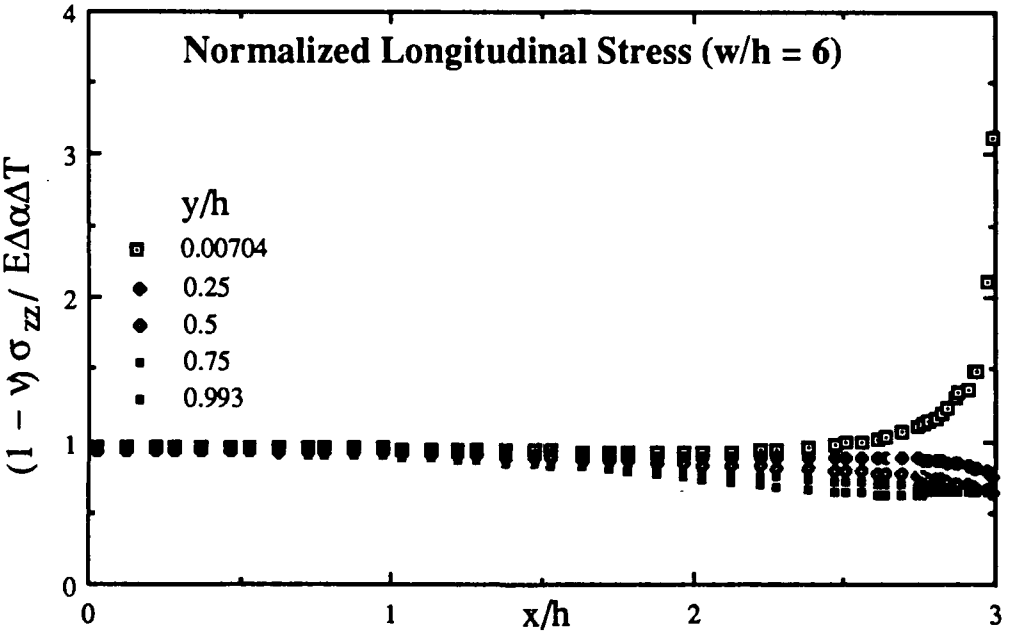

Figure 4(d) Normalized longitudinal stress at various y/h values for an aspect ratio of w/h=6. The normalization factor in all cases is [E/(1-ν)]ΔαΔT. All of these stresses are calculated under plane strain conditions.

Figure 5 shows a comparison of the transverse, normal and shear stresses at y/h = 0.5 for the five different aspect ratios. The transverse stress clearly gets closer to the normalizing value as the aspect ratio is increased; this is to be expected, as a wider line more closely approximates a film than does a narrow line. Also, it can be seen that the percentage of the line across which the stress is approximately constant increases with line width, being around 25% for the w/h = 2 line and closer to 50% for the w/h = 10 line. It is evident that for the normal stress the influence of the edge extends about one line height into the line, so that for the w/h = 2 line, the normal stress varies greatly across the whole line, whereas for the w/h = 10 aspect ratio line the stress is approximately constant and close to zero between x/h = 0 and x/h = 4 , and there is only significant variation between x/h = 4 and x/h = 5. Also note that the maximum value of the normal stress does not change for aspect ratios greater than w/h = 4. The shear stress variations extend farther into the lines than do the normal stress variations, but again the maximum value of the stress does not change much for the wider lines. The negative values of shear stress are expected, since a compressive thermal strain is imposed.

5. Conclusions

The finite element method has been shown to be an accurate way of calculating stresses in thin film structures. Furthermore, while a fairly simple geometry was used in this paper, it would not be difficult to extend the method to complicated structures and to include passivations and compliant substrates. Numerical solutions to problems of this sort would be extremely cumbersome.

It has been shown that as line widths decrease, thermal stresses vary across larger percentages of the line, so that for a w/h = 2 line the stress cannot be taken as constant across any of the line. The current frontiers of integrated circuit technology require smaller and smaller line widths, so it is ever more important to learn about the stresses in these lines. The current calculations should provide useful information about the distribution of these stresses.

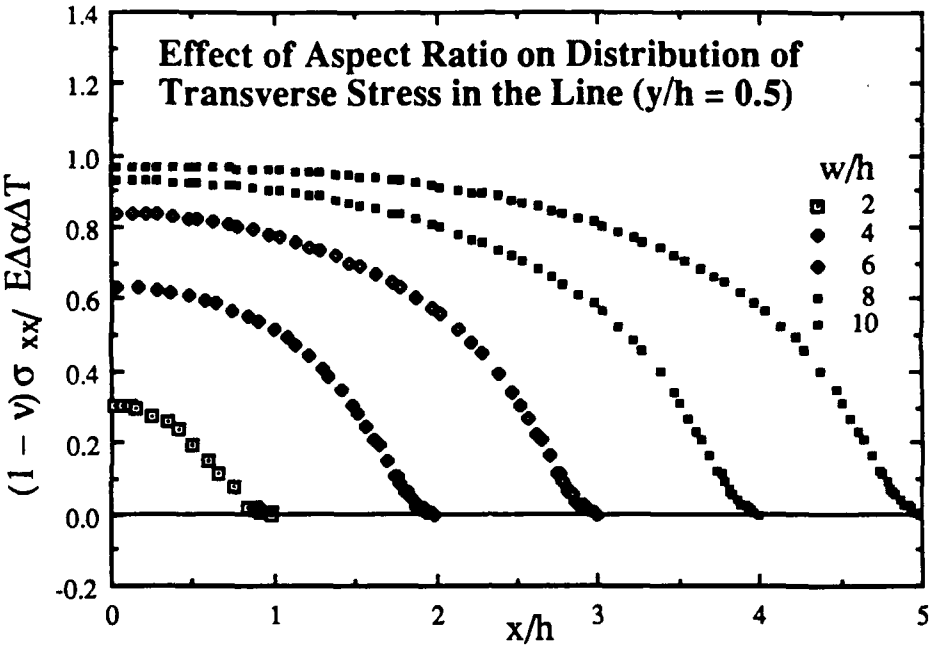

Figure 5(a). Comparisons of transverse stresses at y/h = 0.5 for five different aspect ratios.

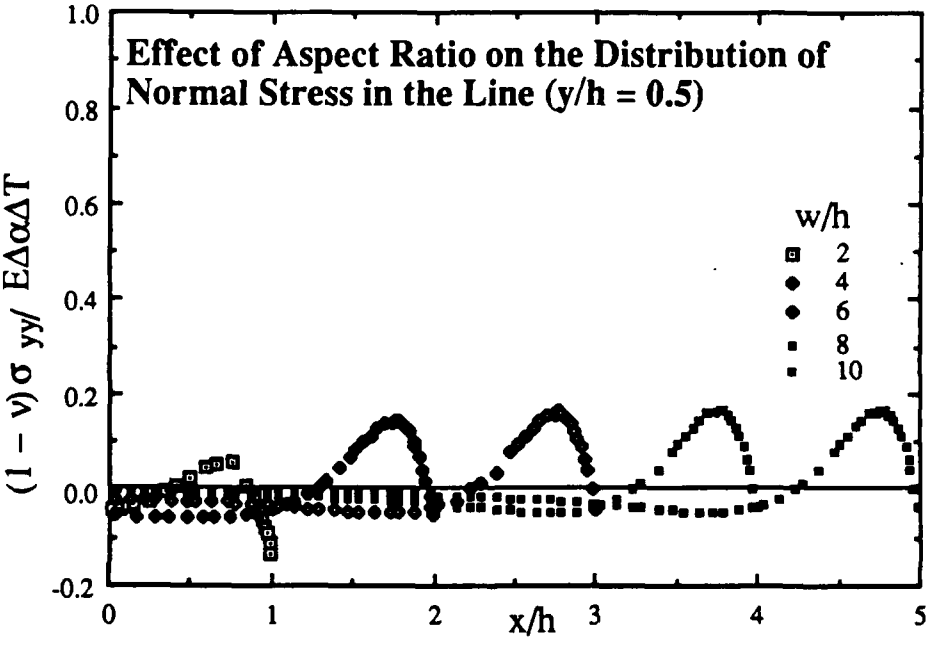

Figure 5(b). Comparisons of normal stresses at y/h = 0.5 for five different aspect ratios.

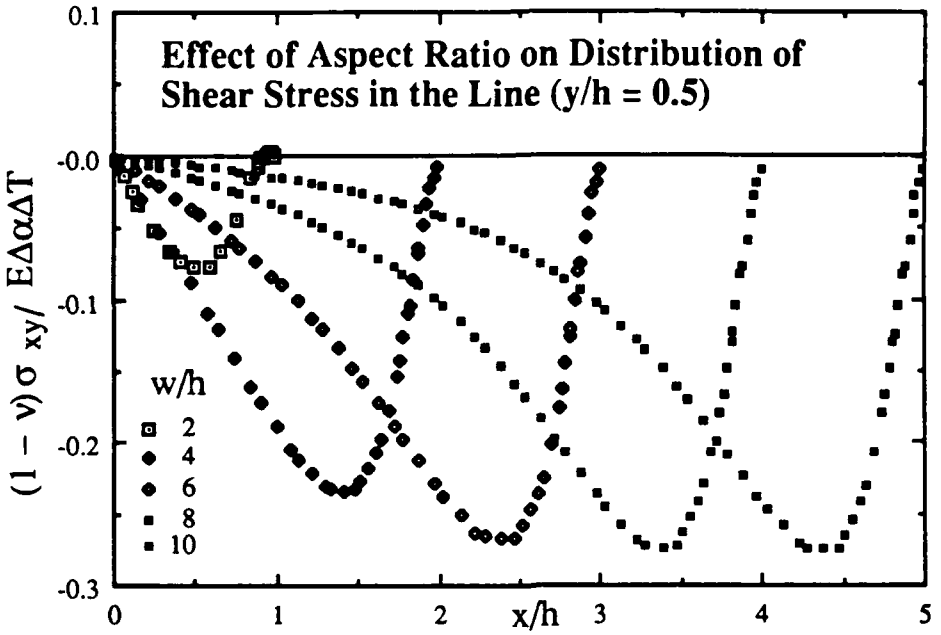

Figure 5(a). Comparisons of shear stresses at y/h = 0.5 for five different aspect ratios.

References

1. R.E. Jones Jr., Proc. IEEE IRPS, 25, 9, (1987).

2. B.J. Aleck, J. Appl. Mech., 16, 118, (1949).

3. I.A. Blech and A.A. Levi, J. Appl. Mech, 48, 442, (1981).

4. D.M. Barnett, Private communication, Stanford University, (1988).

5. M. Murakami, T.S. Kuan and I.A. Blech, in "Treatise on Materials Science and Technology," Vol. 24, Academic Press, New York, (1982).

6. R. Zeyfang, Solid State Electron., 14, 1035, (1971).

III. ORAL PRESENTATIONS RESULTING FROM AFOSR GRANT NO. 86-0051

1. W.D. Nix, "Mechanical Properties of Microelectronic Thin Film Materials", CIS Annual Review, Stanford University, March 6, 1986.

2. W.D. Nix, "New Experimental Techniques for the Study of Mechanical Properties of Microelectronic Thin Files", Department of Mechanical Engineering, University of California, Davis, March 13, 1986.

3. W.D. Nix, Mechanical Properties of Thin Films and Other Fine Scale Structures", Albuquerque Chapter of ASM, Albuquerque, New Mexico, March 19, 1986.

4. M.F. Doerner, "Mechanical Properties of Thin Films Using Nanoindenter Techniques", Materials Science Industrial Affiliates Program, Stanford University, May 28, 1986.

5. M.F. Doerner and W.D. Nix, "Mechanical Properties of Thin Films on Substrates", Micromechanics Research Group, IBM Research Laboratory, San Jose, California, June 27, 1986.

6. W.D. Nix and M.F. Doerner, "Mechanical Properties of Microelectronic Thin Film Materials: Nanoindenter and Wafer Curvature Techniques", Summer Research Group, Materials Science Center, Los Alamos National Laboratory, August 18, 1986.

7. W. D. Nix, "Mechanical Properties of Thin Films", Materials Science Colloquium, Department of Materials Science and Engineering, Stanford University, December 5, 1986.

8. W. D. Nix, "New Experimental Techniques for the Study of Mechanical Properties of Thin Films", Department of Metallurgical Engineering, The Ohio State University, Columbus, Ohio, February 6, 1987.

9. W.D. Nix, "Mechanical Properties of Thin Films", Department of Materials Science, Ecole Polytechnique de Federale Lausanne, Lausanne, Switzerland, April 15, 1987.

10. M.F. Doerner, "Mechanical Properties of Thin Films Using Sub-Micron Indentation Techniques", TMS Fall Meeting, Cincinnati, October 1987.

11. M.F. Doerner, "Stresses and Deformation Processes in Thin Films on Substrates", TMS Annual Meeting, Phoenix, Arizona, January 1988.

12. W.D. Nix, "Mechanical Properties of Thin Films", Intsitute of Metals Lecture, TMS Annual Meeting, Phoenix, Arizona, January 1988.

13. W.D. Nix, "Mechanical Properties of Thin Films and Other Finely Structured Materials", Micrometallurgy 88, TMS Northern California Meeting, Lake Tahoe, California, March 1988.

IV. PUBLICATIONS RESULTING FROM AFOSR GRANT NO. 86-0051

1. D.-B. Kao, J.P. McVittie, W.D. Nix and K.C. Saraswat, "Two-Dimensional Oxidation: Experiments and Theory", Proceedings of IEDM 85, IEEE, 1985, p. 388.
(selected as best student paper at the conference)

2. M.F. Doerner and W.D. Nix, "A Method for Interpreting the Data from Depth-Sensing Indentation Instruments", J. Materials Research, 1, 601 (1986).

3. M.F. Doerner, D.S. Gardner and W.D. Nix, "Plastic Properties of Thin Films on Substrates as Measured by Submicron Indentation Hardness and Substrate Curvature Techniques", J. Materials Research, 1, 845 (1986).

4. P.A. Flinn, D.S. Gardner and W.D. Nix, "Measurement and Interpretation of Stress in Aluminum-Based Metallization as a Function of Thermal History", IEEE Trans. on Electron Devices, ED-34, 689 (1987).

5. D.-B. Kao, J.P. McVittie, W.D. Nix and K.C. Saraswat, "Two-Dimensional Thermal Oxidation of Silicon - I. Experiments", IEEE Trans. on Electron Devices, ED-34, 1008 (1987).

6. D.-B. Kao, J.P. McVittie, W.D. Nix and K.C. Saraswat, "Two-Dimensional Thermal Oxidation of Silicon - II. Modelling Stress Effects in Wet Oxides", IEEE Trans. on Electron Devices, ED-35, 25 (1988).

7. M.L. Ovecoglu, M.F. Doerner and W.D. Nix, "Elastic Interactions of Screw Dislocations in Thin Films on Substrates", Acta Metall., 35, 2947 (1987).

8. M.F. Doerner and W.D. Nix, "Stresses and Deformation Processes in Thin Films on Substrates", CRC Critical Reviews of Solid State and Materials Sciences, 14, 225 (1988).

9. M.F. Doerner and S. Brennan, Strain Distribution in Thin Aluminum Films using X-Ray Depth Profiling", J. Appl. Phys., (1988).